THE JOURNAL OF BIOLOGICAL CHEMISTRY VOL. 289, NO. 10, pp. 6709–6726, March 7, 2014

A Large Scale Huntingtin Protein Interaction Network Implicates Rho GTPase Signaling Pathways in Huntington Disease*[S]◆

Received for publication, October 5, 2013, and in revised form, December 17, 2013 Published, JBC Papers in Press, January 9, 2014, DOI 10.1074/jbc.M113.523696

Cendrine Tourette[‡], Biao Li[‡], Russell Bell[§¶], Shannon O'Hare[‡], Linda S. Kaltenbach[§‖], Sean D. Mooney[‡1], and Robert E. Hughes[‡2]

From the [‡]Buck Institute for Research on Aging, Novato, California 94945, [§]Prolexys Pharmaceuticals, Salt Lake City, Utah 84116, the [¶]Huntsman Cancer Institute, University of Utah, Salt Lake City, Utah 84112, and the [‖]Center for Drug Discovery and Department of Neurobiology, Duke University Medical Center, Durham, North Carolina 27704

Background: Huntington disease is a fatal neuropsychiatric disorder caused by aberrant protein folding and interactions.
Results: An interaction network composed of primary and secondary huntingtin-interacting proteins is significantly enriched for pathways implicated in HD, including RhoGTPases.
Conclusion: Huntingtin interacts with members of the Rho GTPase signaling pathways and regulates filipodial dynamics.
Significance: This protein interaction network provides a resource for HD target discovery.

Huntington disease (HD) is an inherited neurodegenerative disease caused by a CAG expansion in the *HTT* gene. Using yeast two-hybrid methods, we identified a large set of proteins that interact with huntingtin (HTT)-interacting proteins. This network, composed of HTT-interacting proteins (HIPs) and proteins interacting with these primary nodes, contains 3235 interactions among 2141 highly interconnected proteins. Analysis of functional annotations of these proteins indicates that primary and secondary HIPs are enriched in pathways implicated in HD, including mammalian target of rapamycin, Rho GTPase signaling, and oxidative stress response. To validate roles for HIPs in mutant HTT toxicity, we show that the Rho GTPase signaling components, BAIAP2, EZR, PIK3R1, PAK2, and RAC1, are modifiers of mutant HTT toxicity. We also demonstrate that Htt co-localizes with BAIAP2 in filopodia and that mutant HTT interferes with filopodial dynamics. These data indicate that HTT is involved directly in membrane dynamics, cell attachment, and motility. Furthermore, they implicate dysregulation in these pathways as pathological mechanisms in HD.

Huntington disease is an autosomal dominant neurodegenerative disease caused by a CAG repeat expansion in the first exon of the *HTT* gene that encodes the protein huntingtin (HTT) (1). HD[3] manifests with progressive motor and psychiatric impairments caused by neuronal dysfunction and loss in the cortex and striatum (2, 3). Huntingtin is involved in a variety of cellular functions, including vesicle transport, transcription, and energy metabolism (4). HD pathogenesis is generally thought to result from a combination of a gain of toxic properties by mutant HTT as well as a loss of normal huntingtin function (5). Huntingtin is an ~350-kDa protein containing a polyglutamine (polyQ) region, a proline-rich region (PRR), HEAT (Huntingtin, elongation factor 3, protein phosphatase 2A, target of rapamycin 1) repeats, and a number of caspase cleavage sites (4, 6). Several studies have emphasized a critical role of misfolded N-terminal fragments of mutant HTT (7, 8) that are natural products of HTT processing (9). HTT is known to have a large number of interacting proteins involved in a diverse range of biological processes. Numerous studies have shown that polyQ expansion in HTT may alter biological processes that are essential for cellular homeostasis and neuronal survival through impairment of its protein binding activities (10–13).

A number of large scale screens aimed to elucidate new pathways involved in HD pathogenesis by defining HTT partners using yeast two-hybrid (Y2H) and affinity purification approaches (14–17). Analyses of binary interactions or complexes identify the first level of HTT-interacting proteins. We have previously described a protein interaction network derived from a comprehensive Y2H screen using HTT as a bait. That study reported 102 high confidence HTT-interacting proteins, and many of these were shown to be modifiers of mutant HTT toxicity in a *Drosophila* model of HD (16). In this study, we report Y2H screening results for these primary HTT-interacting partners derived from a genome-scale interaction map

* This work was supported, in whole or in part, by National Institutes of Health Grants NS055247 and GM084432 (to R. E. H.). This work was also supported by a grant from CHDI Foundation Inc. (to R. E. H.).
◆ This article was selected as a Paper of the Week.
[S] This article contains supplemental Tables S1–S5.
[1] Supported by National Institutes of Health Grant LM009722, National Center for Biomedical Ontology Grant U54-HG004028, and the CHDI Foundation Inc. To whom correspondence may be addressed: The Buck Institute for Research on Aging, 8001 Redwood Blvd., Novato, CA 94945. Tel.: 415-209-2038; Fax: 415-493-3640; E-mail: smooney@buckinstitute.org.
[2] To whom correspondence may be addressed: The Buck Institute for Research on Aging, 8001 Redwood Blvd., Novato, CA 94945. Tel.: 415-209-2069; Fax: 415-209-2235; E-mail: rhughes@buckinstitute.org.

[3] The abbreviations used are: HD, Huntington disease; HIP, huntingtin-interacting protein; HPRD, Human Protein Resource Database; IPA, ingenuity pathway analysis; Y2H, yeast two-hybrid; HDNet, huntingtin protein interaction network; PRR, proline-rich region; SH, Src homology; BAR, Bin-Amphiphysin-Rvs; PPI, protein-protein interaction; ILK, integrin-linked kinase; RAR, retinoic acid receptor.

(18, 19). Using the 102 HTT primary partners identified in our first screen, we identified a secondary interactome of 2038 known partners to build an expanded huntingtin protein interaction network (HDNet). This network includes HTT-primary, primary-primary, and primary-secondary interacting proteins. We analyzed the connectivity properties of these proteins at the two levels, showing significantly high interconnectivity between HDNet members compared with random proteins in a global curated interaction network from Human Protein Resource Database (HPRD).

Integration of data from different "omics" approaches has been shown to improve functional annotations and to help to formulate biological hypotheses (20). Combination of biological annotations with integration of gene expression data from post-mortem HD brain highlighted the role of Rho family GTPase signaling proteins in HD pathology. Using cell models, we showed that components of this pathway are modifiers of expanded polyQ-induced toxicity. We also showed that mutant HTT interferes with BAIAP2-induced filopodia formation, validating the role of Rho signaling in mutant HTT toxicity. Our study provides a comprehensive resource of binary protein interactions that define novel pathways contributing to Huntington disease pathology.

EXPERIMENTAL PROCEDURES

Y2H Screen—Y2H screens were performed as described previously (21). The screen for primary HTT partners has been described in Kaltenbach *et al.* (16). Interactions of primary partners have been extracted from a genome-wide Y2H screen as described previously (18). Y2H screens were performed in 96-well plates by mating in each well 5×10^6 cells of a yeast clone expressing a single bait with 5×10^6 clonally diverse cells from a prey library. After mating overnight, the matings were plated onto medium that was selected simultaneously for the mating event, the expression of the ORF selection markers, and the activity of the metabolic reporter genes *ADE2* and *HIS3*. Yeast that grew on this selection medium ("positives") were counted and transferred into liquid medium in a 96-well format. Cloned inserts were amplified from plasmid PCR. Liquid cultures grown from positive yeast colonies were used as templates in PCRs that amplified either both bait and prey cDNA inserts or prey inserts only in screens where the baits had been sequenced before the matings.

To determine identity of the coding genes from which the primary and secondary sequence fragments were derived, we first aligned cDNA fragments to the set of human RNA sequences downloaded from NCBI (ncbi.nih.gov). All Y2H search data and DNA sequences used to determine interaction pairs reported in this study are included in supplemental Table S2.

Network Topology Analysis—HTT primary and secondary proteins were anchored to the PPI network defined by HPRD (Release 9). The shortest distances between any two nodes in the PPI network were computed through the Matlab package MATLAB BGL. The largest subgraph contains 9219 proteins, and 64 primary and 1167 secondary proteins could be found in this subgraph, respectively. All network metrics were based on this largest subgraph. To approximate the distribution of the shortest distance observed in HPRD, we randomly sampled 1 million networks with each having 64 nodes as controls to the primary proteins, and 100,000 networks with each having 1167 nodes as controls to the secondary proteins.

Functional Annotation of the Network—Total data set and the subgroups of primary and secondary partners of HTT were analyzed using Ingenuity Pathway Knowledge Base (Ingenuity System, Mountain View, CA). The three groups were subjected to IPA Core analysis. Canonical pathways were considered as significantly enriched with a false discovery rate corrected p value of <0.01. Enriched canonical pathways were ranked based on the corrected p value obtained for the whole HDNet dataset and were represented using the IPA comparison analysis tool. The most significantly enriched lists were visualized in Cytoscape (22), using a union of HDNet and HPRD networks (23). Proteins were represented using node color for HD dysregulation data (24, 25) based on significance level (corrected p value of <0.01) and node shape for level of interaction with HTT (primary/secondary). Edges were represented as lines and dashed lines based on the source of interaction, HDNet and HPRD respectively. Only connected nodes are represented in Figs. 4 and 5 for better visibility; information of all nodes is found in supplemental Table S4.

Domain Identification—The mapped protein segments were searched against NCBI conserved domain database (version 3.05) to obtain domain information, with settings of *E*-value cutoff of 0.01 and filtering low complexity regions. Whenever multiple domains were found on the same protein segments, only the most specific hits were kept. By definitions from the conserved domain database, the specificity of hits decreases in the order of specific domain, superfamily, and multiple domains.

Plasmids, siRNA, and Lentiviruses—BAIAP2 cDNA was obtained from Open Biosystems (MHS1011-59012), PCR-amplified with Pfu Turbo (Agilent) as recommended by manufacturer, with the following primers: forward primer, 5′-CACCATGGCTCTGTCTCGCTC-3′, and reverse primer, 5′-TGGCCATCTGCTGAGGAG-3′. cDNA was next cloned into the Gateway pENTR-D-TOPO vector; C-terminal V5-tagged BAIAP2 was generated by LR reaction with pDEST40 following the manufacturer's protocol (Invitrogen). Clones were verified with sequencing at all the steps. pDEST40-LacZ was used as a negative control. Entry clones containing HTT N-terminal fragments 1–558 (with 23Q or 135Q) fused to a C-terminal GFP tag have been described previously (26). LR reaction was performed with pLenti CMV Puro DEST vector (w118-1, Addgene); integrity of clones and length of CAG repeats were verified by sequencing at all steps. Lentiviral production and infection were performed in HEK293FT as described previously (27). Full-length HTT plasmids were described previously (28). Dharmacon siGENOME SMARTpools (Thermo Scientific) were used for siRNA disruption of CASP3 (M-043042), BAIAP2 (M-046696), EZR (M-046568), PI3KR1 (M-041079), PIK3R2 (M-041085), PIK3R3 (M-041300), PAK2 (M-040615), WAVE (M-061823), and RAC1 (M-041170) using nontargeting pool (D-001206) as a control.

Cell Culture and Transfection—Mouse striatal cell lines expressing full-length HTT with either wild-type (7Q/7Q) or mutant (111Q/111Q) polyglutamines were handled as

described previously (29), maintained at 33 °C in a humidified atmosphere of 95% air and 5% CO_2 in DMEM containing 10% FBS, 100 units/ml penicillin, and 100 μg/ml streptomycin. Cells were nucleofected using kit L (Amaxa) with 3 μg of siRNA for two million cells, as described previously (28). Mouse NIH-3T3 and human HEK293T cells were maintained at 37 °C in a humidified atmosphere of 95% air and 5% CO_2 in DMEM containing 10% FBS, 100 units/ml penicillin, and 100 μg/ml streptomycin. Infection of HEK293T cells was performed as described previously (27). Cells were selected with puromycin (Invitrogen) at a concentration of 1 μg/ml culture media 48 h after infection. NIH-3T3 and HEK293T cells were transfected using Lipofectamine 2000 reagent following the manufacturer's protocol (Invitrogen), with full-length HTT-17Q and HTT-138Q, C-terminal V5-tagged BAIAP2, or Dharmacon smart pool BAIAP2 siRNA.

Caspase Assays—Cell death assays were performed as described previously (28). Briefly, transfected cells were plated on collagen-treated 96-well plates and incubated for 48 h. After 24 h of serum starvation, activation of caspase 3/7 was measured in cells using Apo 3/7 HTS high throughput screen assay kit (Cell Technology), using Fusion Alpha-FP HT (PerkinElmer Life Sciences) microplate reader with excitation and emission wavelengths of 420 and 520 nm, respectively. Toxicity is represented as caspase 3/7 activity in change in relative fluorescence units/min/mg of protein, relative to ST*Hdh*$^{111Q/111Q}$ treated with nontargeting siRNA pool. Tests were performed in triplicates; *t* test was used for statistical analysis (GraphPad Prism).

Western Blotting and Co-immunoprecipitation—Cells were seeded on 6-well plates, harvested, and lysed with M-PER (Thermo Scientific) 72 h after transfection for Western blotting. Primary antibodies anti-BAIAP2, PIK3R1 (Genscript), Ezrin, PAK2 (Cell Signaling), PIK3R2 and PIK3R3 (R&D Systems), RAC1 (Sigma), WASF1 (Upstate), HTT (Millipore), and β-actin (Sigma) were used for protein level quantification and normalization following the manufacturers' protocols. Cells were seeded on 6-well plates, harvested, and lysed with RIPA buffer (50 mM Tris-HCl, pH 7.4, 150 mM NaCl, 1 mM EDTA, 1% Nonidet P-40, 1% sodium deoxycholic acid, 0.1% SDS, protease and phosphatase inhibitors) 48 h after transfection for co-immunoprecipitation. For V5-tagged protein immunoprecipitation, lysates were incubated with anti-V5-agarose affinity gel for 90 min and washed three times in RIPA buffer following the manufacturer's protocol (Sigma). For GFP-tagged precipitation, lysates were pre-cleared with protein G-Sepharose beads (GE Healthcare) for 1 h, incubated overnight with GFP antibody (mouse, Covance), and incubated with protein G-Sepharose beads for 1 h before three washes with RIPA buffer. All steps were performed at 4 °C. Antibodies used for detection of tagged proteins were anti-V5 (Invitrogen), anti-GFP (Cell Signaling).

Immunofluorescence and Filopodia Counting—NIH-3T3 were plated on poly-L-lysine eight-chamber slides (BD Biosciences). 48 h after transfection, cells were rinsed once with 1× PBS and fixed with 4% paraformaldehyde for 10 min and permeabilized with 0.2% Triton X-100 for 2 min. After 30 min of incubation in blocking solution (5% normal donkey serum in PBS), cells were incubated overnight at 4 °C with anti-HTT (Millipore) and anti-V5 (invitrogen) primary antibodies. After incubation with respective secondary antibodies coupled with Alexa Fluor 488 and 647 (Invitrogen) for 1 h at room temperature, cells were incubated with rhodamine-phalloidin coupled with Alexa Fluor 555 (Invitrogen) for 20 min at room temperature to detect filamentous actin. Cells were washed three times with PBS and mounted using Prolong Gold with DAPI (Invitrogen). 15 cells per experiment were imaged using the confocal microscope LSM 780 (Zeiss). Three replicates per condition were performed. Images were analyzed with Zeiss Zen (2011) software; V5- and HTT-positive cells were digitalized using ImageJ process "find edges"; the number of actin-positive filopodia per cell was counted manually for each condition. Number of filopodia per cell was expressed as relative value compared with average filopodia number in control cells. Filopodia were double counted by a blinded experimenter. *t* test was used for statistical analysis (GraphPad Prism). Co-localization experiments were performed using the same methods and materials.

RESULTS

Network Properties of Huntingtin-interacting Proteins in HDNet—We had previously performed two large scale screens to identify novel HTT-interacting proteins using Y2H and mass spectrometry-based methods (16). For the Y2H screen, polyQ containing HTT fragment baits of amino acids 1–90, 1–450, or 1–740 were screened in both wild-type (23Q) and mutant (>45Q) forms against multiple prey libraries generated from human cDNA. Stringent criteria have been used to define high confidence core dataset composed of 102 direct HIPs. We then extracted interaction data for these 102 HIPs to include secondary interacting proteins. This resulted in a network containing 2141 nodes as follows: HTT, 102 primary and 2038 secondary interacting proteins connected through 3235 edges. These edges include 102 interactions of primaries with HTT, 51 primary-primary interactions, and 3082 primary-secondary interactions, representing data obtained from 9423 individual Y2H-positive yeast colonies (Fig. 1 and supplemental Tables S1 and S2). We refer to this network as HDNet.

HDNet is centered on HTT with two levels of partners and includes interactions between primary nodes (Fig. 1*B*). Because we do not have information about interactions between secondary nodes, the network does not have a scale-free topology. To characterize the connectivity properties of HDNet members in the context of a scale-free network, we mapped HTT primary and secondary partners in the curated large scale HPRD protein interaction network (HPRD Release 9) (23). We then calculated the shortest path among them, using the literature-curated interactions described in HPRD. With nodes defined according to Entrez Gene IDs, 79 out of 102 primary and 1408 out of 2038 secondary interacting proteins were present in the largest sub-network in HPRD, which consists of 8783 of the total 9019 proteins (Fig. 2*A*).

This analysis showed that both primary and secondary proteins present in HDNet have significantly higher average node degrees as compared with the average for HPRD as a whole (18.25 and 10.80 *versus* 7.63, both p value < 0.001). This is true for median node degrees as well, indicating that the high connectivity of HDNet proteins in HPRD is not due to the presence of highly connected outliers (Fig. 2, *A* and *B*). The average

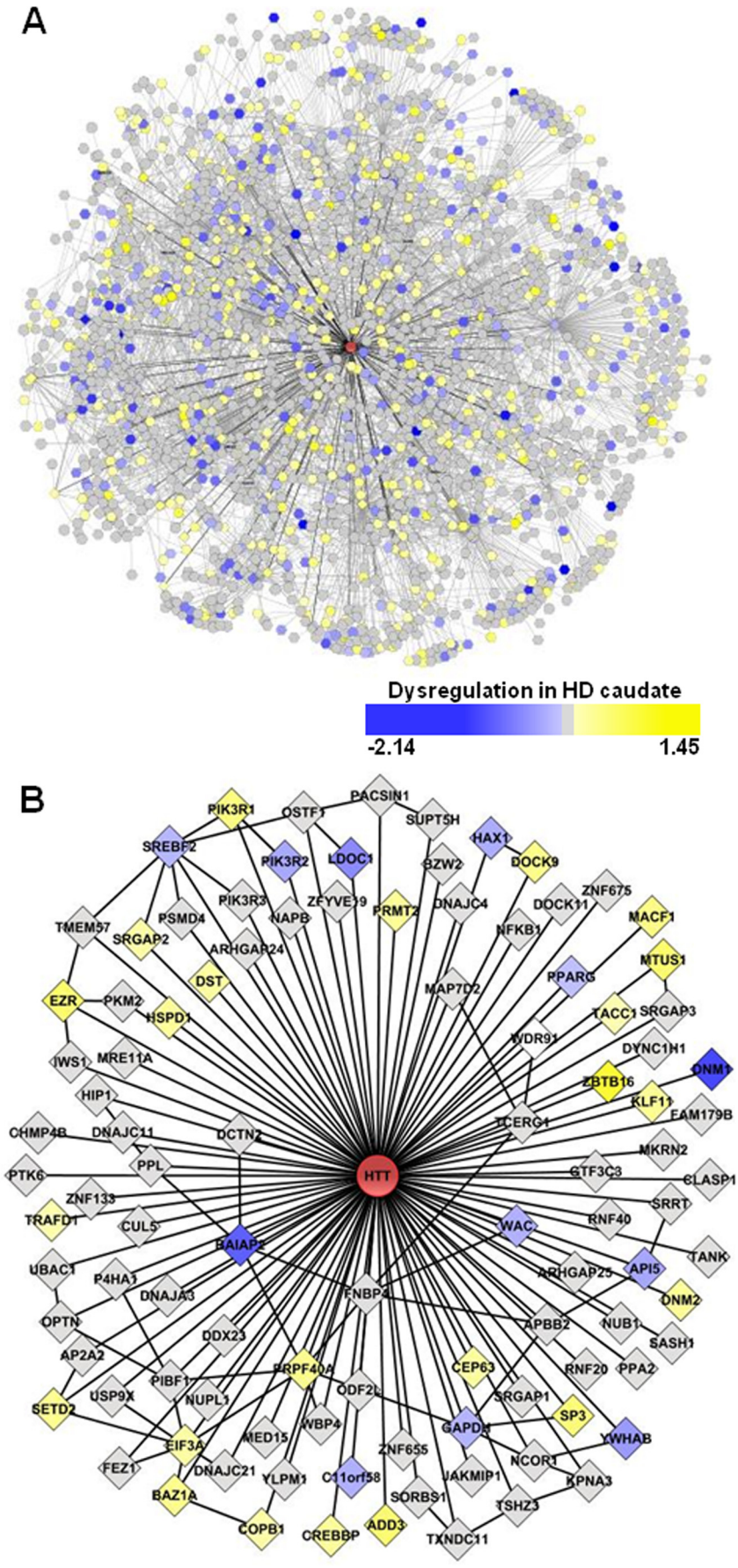
A
Dysregulation in HD caudate
-2.14
1.45
B
HTT
PACSIN1
PIK3R1
OSTF1
SUPT5H
HAX1
SREBF2
PIK3R2
LDOC1
BZW2
DOCK9
PIK3R3
ZFYVE19
PRMT2
DNAJC4
DOCK11
ZNF675
TMEM57
PSMD4
NAPB
NFKB1
MACF1
SRGAP2
ARHGAP24
MTUS1
DST
PPARG
EZR
PKM2
MAP7D2
HSPD1
TACC1
SRGAP3
VDR91
IWS1
MRE11A
DYNC1H1
DNM1
HIP1
ZBTB16
KLF11
FAM179B
CHMP4B
DNAJC11
DCTN2
TCERG1
MKRN2
PTK6
PPL
GTF3C3
CLASP1
ZNF133
SRRT
TRAFD1
CUL5
RNF40
WAC
BAIAP2
TANK
UBAC1
P4HA1
ARHGAP25
API5
DNAJA3
FNBP2
DNM2
OPTN
APBB2
NUB1
DDX23
SASH1
AP2A2
CEP63
RNF20
PPA2
PRPF40A
PIBF1
ODF2L
SRGAP1
USP9X
SP3
SETD2
NUPL1
GAPDH
YWHAB
WBP4
MED15
EIF3A
ZNF655
NCOR1
FEZ1
DNAJC21
YLPM1
C11orf58
JAKMIP1
KPNA3
BAZ1A
SORBS1
TSHZ3
COPB1
CREBBP
ADD3
TXNDC11

shortest path lengths among both primary (3.39) and secondary HIPs (3.87) are significantly shorter than that observed in HPRD as a whole (4.25; Fig. 2, *C* and *D*; both p value $<2.2e\text{-}16$; t test). The significantly higher connectivity observed among HDNet primary and secondary nodes within the HPRD background suggests that these groups of proteins are enriched for shared functions and/or membership in common biological pathways (30). However, high node degrees could also contribute to short path lengths between nodes. We thus analyzed the properties of randomly generated networks to determine whether this was the case. We first tested if the number of proteins in each group influenced the respective connectivity. We selected random cohorts of proteins with population sizes of HDNet primary (79) or secondary (1408) interactors from HPRD and calculated the average shortest path lengths for these. This process was repeated 10^6 times for the primary cohort simulation and 10^5 times for the secondary cohort simulation. In both cases, the shortest path length distributions were very similar to the HPRD as a whole, ~4.25 in both cases (data not shown). Given that nodes in HDNet have a higher average node degree as compared with HPRD, we wanted to determine how this property might contribute to the shorter path lengths observed between primary and secondary HIPs in HPRD. To do this, we repeated the simulation with randomly selected cohorts as described above but preserved the node degree distributions of the primary and secondary nodes. These simulations were performed 10^4 times in each case. We observed that sub-networks simulated this way are less interconnected than either primaries or secondaries (Fig. 2, *C* and *D*, respectively).

Analyses of the network properties of primary and secondary nodes in HPRD indicate that HIPs identified in our Y2H screen tend to have higher node degrees and tend to be more highly interconnected. In both cases, these differences are statistically significant. The high degree of interconnectedness of HDNet proteins in the independently derived and curated HPRD protein interaction network indicates that these proteins have shared properties and are likely to participate in shared biological functions. The increased node degree distribution observed among HIPs also indicates that the HTT network is enriched for highly connected proteins.

Functional Analysis of HDNet—Functional analysis of HDNet was performed using the IPA tool (Ingenuity System Inc.). We found that 51 canonical pathways were significantly enriched (B–H, p value = or <0.01) among HDNet proteins (supplemental Table S3). The 20 most significant canonical pathways enriched in HDNet are shown in Fig. 3*A*. Analyses were also performed separately with either primary or secondary nodes alone. This was done to determine the relative contribution of each category of partners (direct and indirect) to pathway enrichments, as well as to uncover potential bias due to an overlap between our dataset and HTT-interacting proteins curated in the IPA knowledge base. Notably, the fourth most significantly enriched canonical pathway in HDNet is Huntington disease signaling. Some of the proteins in this pathway have been reported as HIPs and have been validated in multiple sources (16). Interestingly, HD signaling is also significantly enriched in secondary interaction partners. These results further validate the biological significance of HDNet.

The top three most significantly enriched pathways revealed by IPA analysis are related to protein synthesis and protein homeostasis as follows: EIF2, EIF4, p70S6K, and mammalian target of rapamycin signaling pathways (Fig. 3*A*). Primary HTT partners like PIK3R1, -2, and -3 (phosphoinositide 3-kinase regulatory) subunits and EIF3A (eukaryotic elongation factor 3 member A), as well as secondary partners like EIF and ribosomal proteins S and L family members are represented in all these canonical pathways (supplemental Table S3). Notably, PIK3R family members are present in a number of enriched pathways. Dysregulation of the PI3K pathway is associated with numerous cancers (31), inflammatory diseases (32), and metabolic diseases like diabetes (33). This pathway has also been shown to play a critical role in neurodegenerative diseases such as HD (34, 35).

Four other enriched canonical pathways are determined mainly by primary interacting partners as follows: NRF2-mediated oxidative stress response; aldosterone signaling in epithelial cells; clathrin-mediated endocytosis signaling, and retinoic acid receptor activation. NRF2, aldosterone, and retinoic acid receptor signaling pathway findings highlight the transcriptional role of HTT and its dysregulation in HD (36). The clathrin-mediated endocytosis pathway is known to be affected by mutant HTT (37, 38). Our data from primary and secondary interacting partners indicate that multiple components of these pathways interact with mutant HTT.

Enriched pathways driven by the secondary partners provide a broader view of global signaling pathways potentially impacted by HTT. These include the following: Rho family GTPase, actin cytoskeleton, and integrin-linked kinase signaling as well as molecular mechanisms of cancer. Interestingly, Rho family GTPase signaling is enriched in the secondary partner set, with Rho family, RHOA, and ARHGDI (RHOGDI), sharing components with actin signaling and integrin-linked kinase pathways. These canonical pathways are all involved in cell migration, adhesion, proliferation, and signal transduction (39, 40). Members of ARHGEF (anti-Rho guanine nucleotide-exchange factor), Rho GTPases (ROCK1 and RAC1), myosins and Wiskott-Aldrich syndrome protein families are found as secondary HTT partners. Several studies have showed that Rho GTPases, in particular ROCK1, have an effect on aggregation and degradation of mutant HTT (41, 42). As other components of these pathways have been highlighted independently with our Y2H screen, we suggest that this could also support the known role of HTT in vesicle trafficking as well as novel functions and pathological effects on cell adhesion and cell migration.

FIGURE 1. **HDNet is an HTT interactome composed of primary and secondary interacting proteins.** *A,* network is composed of HTT (*red*), 102 primary partners, and 2038 secondary partners connected though 3235 edges. *B,* first level of HTT-interacting proteins shows HTT-primary and primary-primary interactions. Node colors represent gene expression dysregulation in HD human caudate sample.

A

		HPRD	
		HDNet-1°	HDNet-2°	total
	Nodes	79	1408	9019
	Edges	1439	13337	34409
Node Degree	Average	18.39	10.8	7.63
	SD	16.21	7.15	9.7
	Median	14.62	7.78	3.42

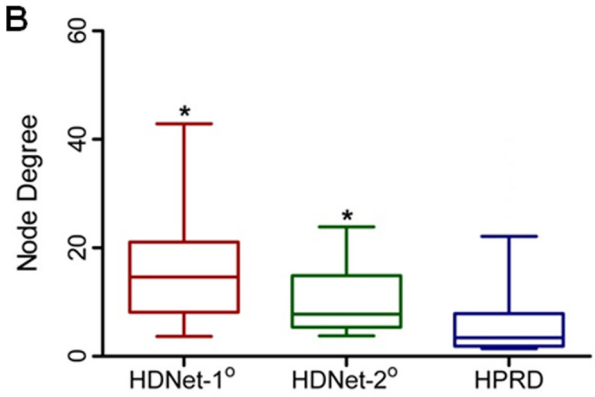

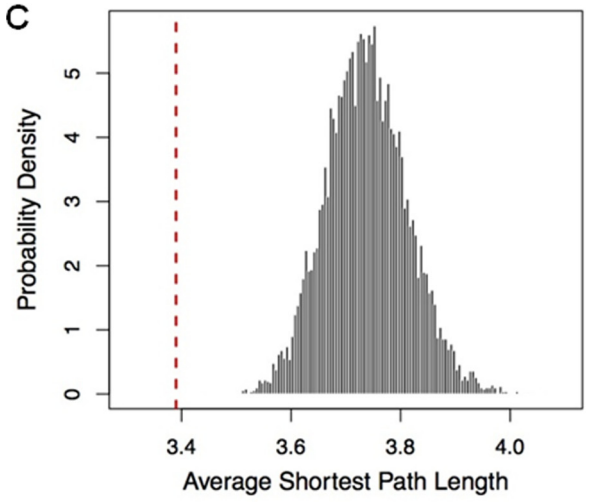

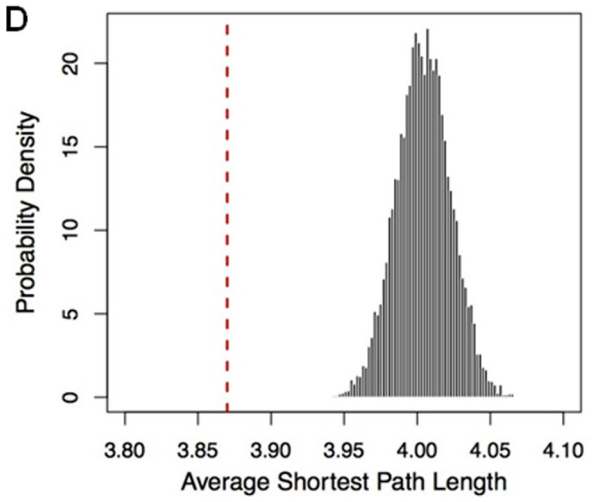

Correlation of HDNet with Transcriptional Dysregulation in HD—Integration of data from different types of genome-scale approaches has been shown to facilitate functional annotation and to help to formulate biological hypotheses (20, 43). To prioritize the exploration of enriched pathways and associated protein networks, we next integrated HDNet pathway cohorts with HD gene expression data. We focused on gene expression dysregulation data in grade 2 HD patient caudate nucleus (24, 25). Because some canonical pathways had significant overlap in gene members, highly similar pathways were combined into composite lists prior to analysis. EIF2, EIF4/p70S6K, and mammalian target of rapamycin signaling (Fig. 3*A*) were grouped into a pathway referred to as "mammalian target of rapamycin EIF2 and EIF4" (Fig. 3*B*). Similarly, Rho family GTPase, RhoA, and RhoGDI (Fig. 3*A*) signalings were grouped into a pathway referred to as "Rho GTPase family" (Fig. 3*B*). We then tested whether canonical pathways identified with ingenuity analysis and grouped pathways were enriched in dysregulated genes identified in HD caudate. Six canonical pathways were found enriched in dysregulated genes as compared with genome as well as genes represented in the entire HDNet dataset (Fig. 3*B*; hypergeometric test, B–H corrected p value < 0.01 and supplemental Table 4). Subnetworks of dysregulated proteins from enriched pathways are shown in Fig. 4. These subnetworks show interconnections based on a combination of HDNet and HPRD data. Subnetworks from canonical pathways without significant enrichment in genes dysregulated in HD caudate are shown Fig. 5. Notably, in this analysis to identify HIPs with dysregulated expression, the Huntington disease signaling pathway showed the highest enrichment of dysregulated genes. This analysis highlighted also the involvement of Rho GTPase family signaling, with a group of proteins found in more than one enriched canonical pathway. These include EZR (Ezrin), BAIAP2 (brain-specific angiogenesis inhibitor 1-associated protein 2), PI3K family members, cAMP-response element-binding protein, and cAMP-response element-binding protein-binding protein (supplemental Table S4 and Fig. 4)

Based on a combination of pathway analysis combined with gene expression data from HD brain, we focused on the Rho GTPase family module. Rho GTPases are involved in numerous cell processes acting downstream of growth factor receptor activation. Exchange of GDP for GTP by guanine exchange factors activates small GTPases and results in binding to their downstream effectors. GTP hydrolysis by GTPase-activating proteins inhibits their function. RhoGDIs (Rho guanine nucleotide-dissociation inhibitors) regulate Rho GTPase activity by disassociating them from plasma membrane (44). Rho GTPases such as RAC1 or CDC42 activate WAVE complexes (nucleation-promoting factors, including WAS, WASL (N-WASP),

FIGURE 2. **Connectivity properties of HDNet.** *A,* distribution of node degrees of HDNet partners in the HPRD network. *B,* average node degrees of primary and secondary partners compared HPRD nodes in HPRD network (with average, S.D., and median, p value <0.001). *, $p < 0.05$. *C,* distribution of average shortest path lengths from HPRD subnetworks with the same node degree distribution as primary partners (*red line* indicates average shortest path length between primary nodes). *D,* distribution of average shortest path lengths from HPRD subnetworks with the same node degree distribution as secondary partners (*red line* indicates average shortest path length between secondary nodes).

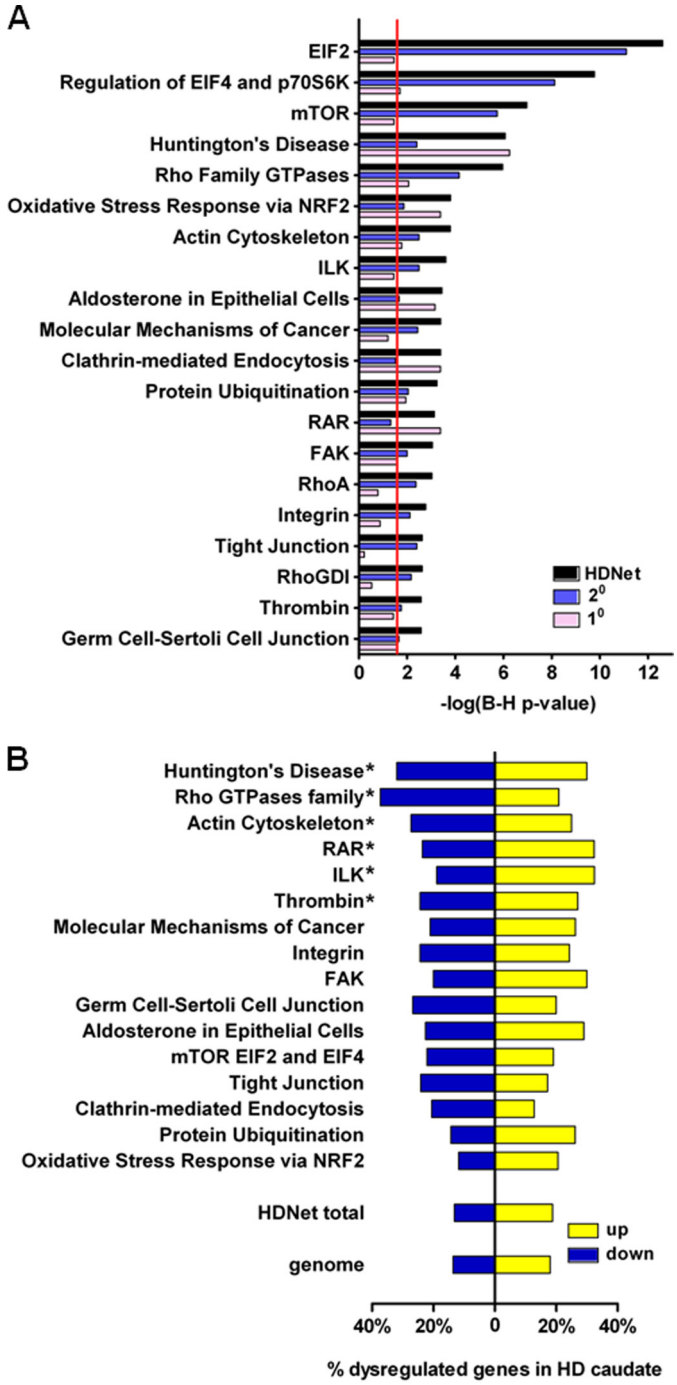

FIGURE 3. **Functional characterization of primary and secondary HTT interaction partners using IPA.** *A,* ingenuity pathway analysis of HDNet members and primary and secondary separately. The 20 most enriched canonical pathways are represented based on whole dataset ranking. *Red line* indicates threshold for significance (B-H corrected, p value = 0.05). *B,* enrichment analysis of IPA functional subgroups for gene expression dysregulation from human HD caudate (log2 fold-change is indicated; *, B-H corrected, p value <0.01).

and WAVE1–3 (WASF1)), which in turn activate Arp2/3 complex, leading to induction of actin polymerization and remodeling of cytoskeletal interactions. Formins, like mDia, protect barbed ends of actin filaments from capping, thereby promoting elongation. Activated RAC1 binds to BAIAP2 to form a protein complex with WAVE to induce membrane ruffling and actin polymerization through Arp2/3 complex (45). Rac also activates PAK proteins, responsible for the delivery of WAVE protein to the plasma membrane. Ena-VASP complexes, anti-capping proteins, are found at the tip of filopodia. BAIAP2 induces filopodia formation through its I-BAR domain (see Table 1 and Fig. 6), inducing cluster formation of phosphatidylinositol 4,5-bisphosphate at the membrane and activating phosphatidylinositol 4,5-bisphosphate-binding proteins such as WASL (46). BAIAP2 activity is inhibited by threonine phosphorylation, leading to 14-3-3 protein binding (47).

EZR is a member of ERM (ezrin, radixin, and moesin) proteins. ERM proteins mediate the attachment of the membrane to actin filaments and are activated by phosphorylation. They are involved in membrane organization and signal transduction (48). Phosphorylated forms of ERM proteins are found at the site of filopodial shafts in axonal growth cones and are dephosphorylated in response to signals that cause growth cone collapse and loss of filopodia (49).

Domain Interactions in HDNet—HDNet is derived from 9423 unbiased observations of individual binary protein interactions (*i.e.* Y2H-positive yeast colonies). Because the bait and prey libraries used in this study were prepared from cDNA fragments, Y2H interactions reported here are between protein fragments. The average insert size in our Y2H libraries is 481 bp (±140 bp). This corresponds to an average protein fragment size of 160 amino acids. We used the conserved domain database (50) to identify conserved domains contained in protein coding regions for both primary and secondary HTT interacting partners. Of these, specific conserved protein domains could be identified in 6541 (35%) activation domain fusions and 3903 (21%) binding domain fusions. In 2268 (12%) cases conserved domains were identified for both activation domain and DNA binding domain in a binary pair (supplemental Table S5). To characterize the domain-domain interaction information in HDNet, we determined frequency of domains present in the protein sequences mediating binary interaction with HTT. Table 1 shows the conserved domains most frequently present in primary partners interacting directly with HTT. Only those domains observed interacting with HTT two or more times are included. The WW domain was found as the most frequent conserved domain interacting with HTT. The WW domain is a short module of 40 amino acids that mediate protein-protein interaction with PRR and thus are likely to interact with the PRR of HTT (51). Binding of TCERG1, APBB members, WBP4, and SETD2 with HTT is known to involve WW-PRR domain interactions (11, 52–54). It has also been shown that interactions involving the PRR of HTT can be affected polyQ expansion (55), indicating potential roles in HD pathogenesis (56). The FF domain was also found at high frequency among primary interactors. Composed of three α-helices, FF domains are present in RNA regulatory proteins and Rho GTPase regulatory proteins and are often found adjacent to WW domains (57, 58). High frequency of interactors with DNA binding domains such as helix-loop-helix and zinc finger domains are consistent with the role of mutant HTT in direct effects causing transcriptional dysregulation (36, 59). Src homology 2 and 3 (SH2 and SH3) domains were also found at high frequency in primary partner sequences responsible for their interaction with HTT. The SH2

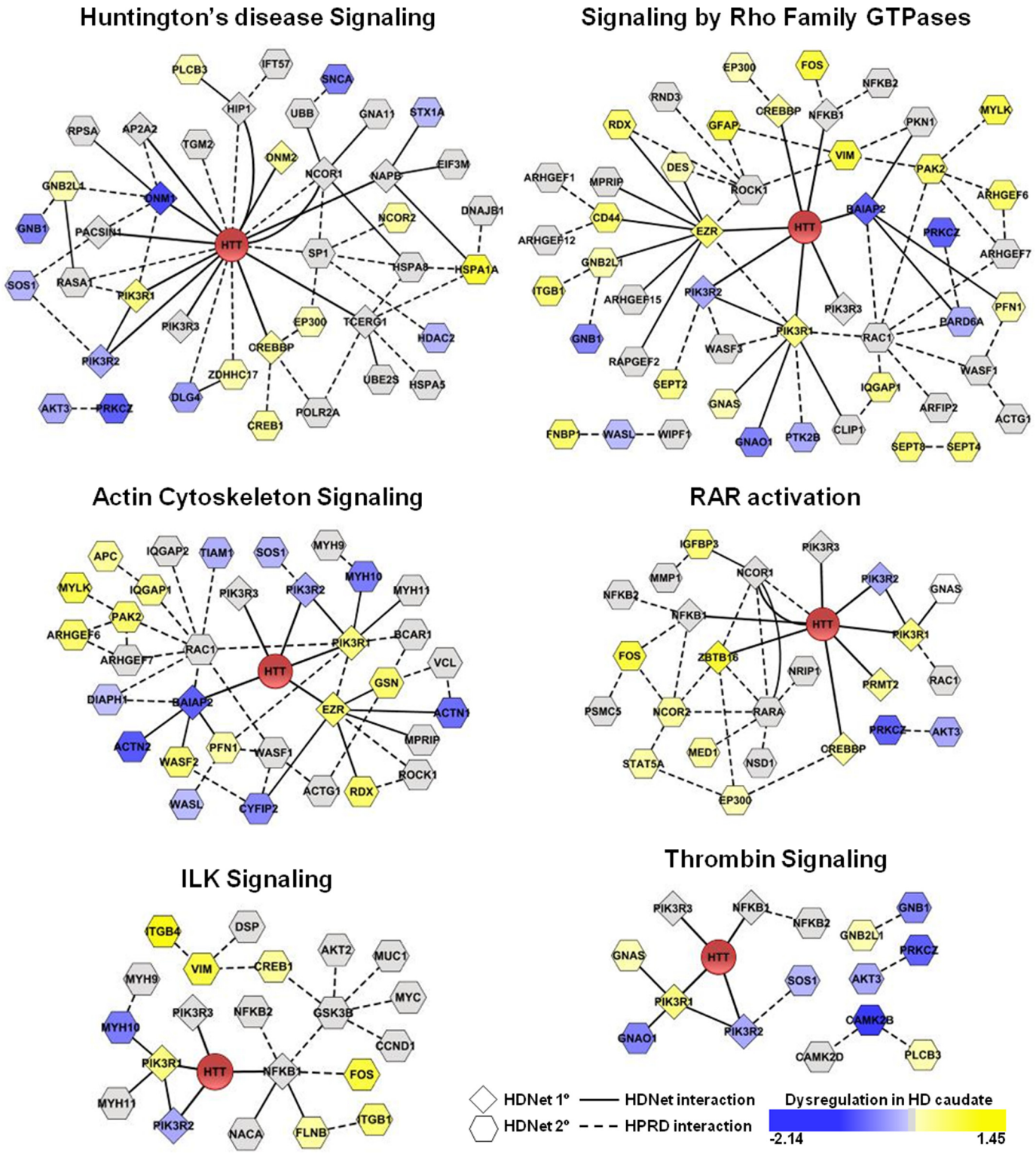

FIGURE 4. **Modules identified by functional and gene expression enrichment analysis.** Functional groups identified using ingenuity pathway and enriched gene expression dysregulation analyses are represented as modules based on a combination of HDNet and HPRD interactions. Node shape indicates the interaction type (*diamond* indicates primary and *hexagon* indicates secondary) with HTT from HDNet data. Node color indicates dysregulation in gene expression (log2 fold-change is indicated; *yellow* indicates increased and *blue* indicates decreased). *Solid lines* indicate interaction from HDNet. *Dashed lines* indicate interactions from HPRD.

domain is mainly found in adaptor proteins and recognizes tyrosine-phosphorylated sites involved in intracellular signaling cascades (60). SH3 domains are also present in adaptor proteins that link partners with their respective PRRs (61). Like the WW domain, SH3 has been implicated in HD pathogenesis through its interaction with the PRR of HTT. Two domain superfamilies are linked to protein degradation, DnaJ and ubiquitin-associated domains. Proteins containing these domains have been implicated in mutant HTT toxicity and clearance of HTT aggregates (62–64).

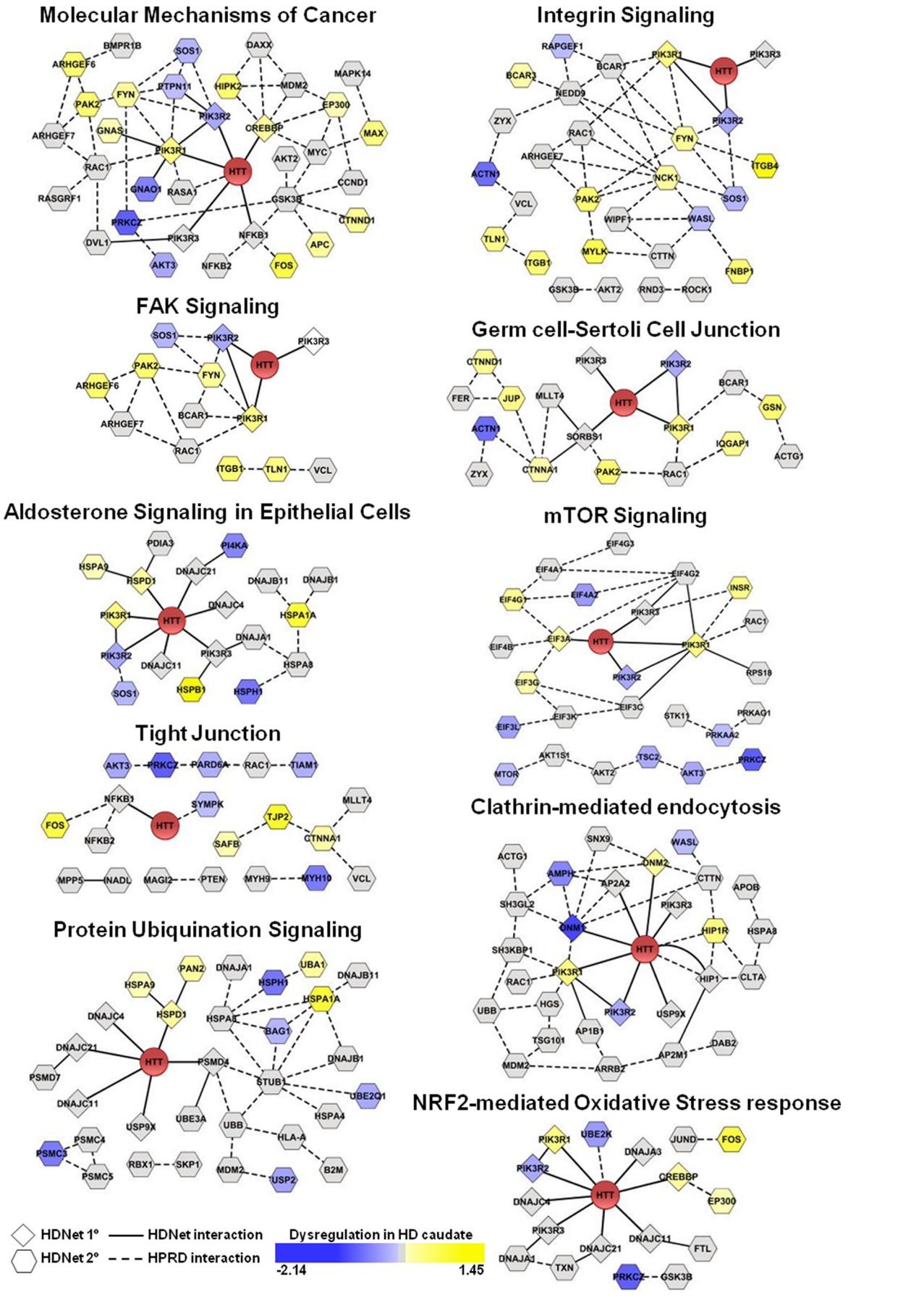
Molecular Mechanisms of Cancer
BMPR1B
SOS1
DAXX
ARHGEF6
PTPN11
HIPK2
MDM2
MAPK14
PAK2
FYN
EP300
PIK3R2
CREBBP
ARHGEF7
GNAS
MAX
PIK3R1
MYC
RAC1
HTT
AKT2
GNAQ
RASA1
CCND1
RASGRF1
GSK3B
PRKCZ
CTNND1
DVL1
PIK3R3
NFKB1
APC
AKT3
NFKB2
FOS
Integrin Signaling
RAPGEF1
PIK3R1
PIK3R3
BCAR1
HTT
BCAR3
NEDD9
ZYX
PIK3R2
RAC1
FYN
ARHGEF7
ITGB4
ACTN1
NCK1
VCL
PAK2
SOS1
WIPF1
WASL
TLN1
MYLK
CTTN
ITGB1
FNBP1
GSK3B
AKT2
RND3
ROCK1
FAK Signaling
SOS1
PIK3R2
PIK3R3
HTT
PAK2
FYN
ARHGEF6
BCAR1
PIK3R1
ARHGEF7
RAC1
ITGB1
TLN1
VCL
Germ cell-Sertoli Cell Junction
CTNND1
PIK3R3
PIK3R2
FER
JUP
MLLT4
HTT
BCAR1
GSN
ACTN1
SORBS1
PIK3R1
IQGAP1
ACTG1
ZYX
CTNNA1
PAK2
RAC1
Aldosterone Signaling in Epithelial Cells
PDIA3
PI4KA
HSPA9
HSPD1
DNAJC21
DNAJB11
DNAJB1
DNAJC4
PIK3R1
HTT
HSPA1A
DNAJA1
PIK3R2
PIK3R3
HSPA8
DNAJC11
SOS1
HSPB1
HSPH1
mTOR Signaling
EIF4G3
EIF4A1
EIF4G2
INSR
EIF4G1
EIF4A2
PIK3R3
RAC1
EIF4B
EIF3A
HTT
PIK3R1
PIK3R2
RPS18
EIF3G
EIF3K
EIF3C
STK11
PRKAG1
EIF3L
PRKAA2
AKT1S1
TSC2
PRKCZ
MTOR
AKT2
AKT3
Tight Junction
AKT3
PRKCZ
PARD6A
RAC1
TIAM1
NFKB1
SYMPK
FOS
HTT
TJP2
MLLT4
NFKB2
SAFB
CTNNA1
MPP5
NADL
MAGI2
PTEN
MYH9
MYH10
VCL
Clathrin-mediated endocytosis
SNX9
WASL
ACTG1
DNM2
AMPH
AP2A2
CTTN
APOB
SH3GL2
PIK3R3
DNM1
HIP1R
HSPA8
SH3KBP1
HTT
RAC1
PIK3R1
HIP1
CLTA
UBB
HGS
PIK3R2
USP9X
TSG101
AP1B1
DAB2
MDM2
ARRB2
AP2M1
Protein Ubiquination Signaling
PAN2
DNAJA1
UBA1
HSPA9
HSPH1
DNAJB11
HSPA1A
DNAJC4
HSPD1
HSPA8
BAG1
DNAJC21
HTT
PSMD4
DNAJB1
PSMD7
STUB1
UBE2Q1
DNAJC11
HSPA4
UBE3A
USP9X
UBB
HLA-A
PSMC4
PSMC3
RBX1
SKP1
MDM2
B2M
PSMC5
USP2
NRF2-mediated Oxidative Stress response
PIK3R1
UBE2K
JUND
FOS
DNAJA3
PIK3R2
CREBBP
HTT
DNAJC4
EP300
PIK3R3
DNAJC11
DNAJC21
FTL
DNAJA1
TXN
PRKCZ
GSK3B
HDNet 1°
HDNet interaction
HDNet 2°
HPRD interaction
Dysregulation in HD caudate
-2.14
1.45

TABLE 1
Conserved domains most frequently observed interacting with huntingtin in the primary network

Domain	Accession	No.	Associated proteins (gene_symbol)
WW superfamily	cl00157	1325	APBB2,TCERG1, WBP4, FNBP4, SETD2, WAC, PRPF40A
FF superfamily	cl02610	170	TCERG1, PRPF40A
zf-H2C2_2 superfamily	cl16282	144	SP3, KLF11, ZNF655, ZNF675
SH2 superfamily	cl15255	132	PIK3R1, PIK3R2, PIK3R3
SH3	cd00174	123	PRMT2, PTK6, SRGAP3, BAIAP2, SORBS1, SRGAP2, OSTF1, SRGAP1
Dynamitin	pfam04912	50	DCTN2
NrdE_NrdA	TIGR02506	46	USP9X
DnaJ	cd06257	43	DNAJC11, DNAJC4, DNAJA3, DNAJC21
Ubiquitin-associated superfamily	cl00153	42	UBAC1, NUB1, OPTN
Pyruvate_kinase superfamily	cl09155	24	PKM
NR_DBD_like superfamily	cl02596	21	PPARG
Snf7 superfamily	cl02305	21	CHMP4B
ARS2 superfamily	cl04863	17	SRRT
ANK	cd00204	16	OSTF1, NFKB1
RhoGAP superfamily	cl02570	16	ARHGAP24, ARHGAP25, SRGAP1
DHR2_DOCK superfamily	cl06123	14	DOCK9, DOCK11
14-3-3 superfamily	cl02098	12	YWHAB
ARM	cd00020	12	KPNA3
Mre11_DNA_bind superfamily	cl04421	12	MRE11A
zf-C2H2_jaz superfamily	cl09952	11	DNAJC21
BAR superfamily	cl12013	10	BAIAP2, PACSIN1
TBD superfamily	cl15118	10	TANK
DDT superfamily	cl02674	7	BAZ1A
VHS_ENTH_ANTH superfamily	cl02544	7	HIP1
P4Ha_N superfamily	cl07084	6	P4HA1
PH-like superfamily	cl00273	6	DNM2, DNM1
SAM_superfamily	cl15755	6	SASH1
TACC	pfam05010	6	TACC1
FEZ superfamily	cl06682	5	FEZ1
zf-CCCH superfamily	cl11592	5	MKRN2
MT superfamily	cl15084	4	DYNC1H1
vWFA superfamily	cl00057	4	PSMD4
API5 superfamily	cl09392	3	API5
HLH	cd00083	3	SREBF2
KRAB_A-box superfamily	cl02581	3	ZNF133
Med15	pfam09606	3	MED15
Adaptin_N	pfam01602	2	AP2A2
BTB superfamily	cl02518	2	ZBTB16
Coatamer_β_C superfamily	cl06658	2	COPB1
CULLIN superfamily	cl10551	2	CUL5
ERM	pfam00769	2	EZR
NGN_Euk	cd09888	2	SUPT5H
PRP40	COG5104	2	PRPF40A, TCERG1
Pyrophosphatase superfamily	cl00217	2	PPA2
RING superfamily	cl15348	2	MKRN2
TPR	cd00189	2	GTF3C3

The presence of domains like RhoGAP and DHR2_DOCK (dock homology region, a guanine exchange factor domain) indicates a potential role of HTT in activity of small GTPases such as RAC1 or CDC42. BAR domain superfamily is responsible for membrane remodeling, invagination or protrusion, in collaboration with nucleation-promoting factors. BAR domain superfamily can be divided into three families, based on structure and functions as follows: N-BAR and F-BAR domains form homodimers that bind concave membrane surface, creating a membrane tubular invagination, whereas the I-BAR domain is responsible for membrane protrusion (*e.g.* lamellipodia/filopodia) (65). These findings are in agreement with results showing enrichments for Rho family GTPases and actin signaling pathways. This analysis adds a new insight into PPI data, more precise resolution for HTT protein interactions at pathway and network levels. As an example, we represented primary partners of Rho GTPase modules (Fig. 6) with their interactions with candidate conserved domains based on our domain analyses. Results showed that BAIAP2 seems to interact mostly through its SH3 domain with HTT. The BAR domain of BAIAP2 is a member of I-BAR, or IMD (IRSp53-MIM homology domain). BAIAP2 interacts through IMD with small GTPases (CDC42, RAC1, and RHOF) and with downstream effectors like EPS8, Mena, and WAVE family members through its SH3 domain for actin remodeling (45, 66–70). Analysis of interactions of the BAR domain of BAIAP2 highlighted PDZ domains present in MAGI (membrane-associated guanylate kinase, WW and PDZ domain containing) and DLG (discs, large homolog), SH3 domain (present in EPS8), and RhoGEF domains (RASGRF1 and FGD5). This is in agreement with the role of BAIAP2 in modulating actin cytoskeleton and membrane protrusion through small GTPases signaling. Domain analysis shows that HTT interacts with the ERM domain of EZR. We also note that all three members of PIK3R subunits

FIGURE 5. **Additional functional modules identified by ingenuity pathway analysis.** Proteins identified using IPA canonical pathways, but not significantly enriched in gene expression dysregulation, are represented as modules based on a combination of HDNet and HPRD interactions. Node shape indicates the interaction type (*diamond* indicates primary and *hexagon* indicates secondary) with HTT from HDNet data. Node color indicates dysregulation in gene expression (log2 fold-change is indicated; *yellow* indicates increased and *blue* indicates decreased). *Solid lines* indicate interaction from HDNet. *Dashed lines* indicate interactions from HPRD.

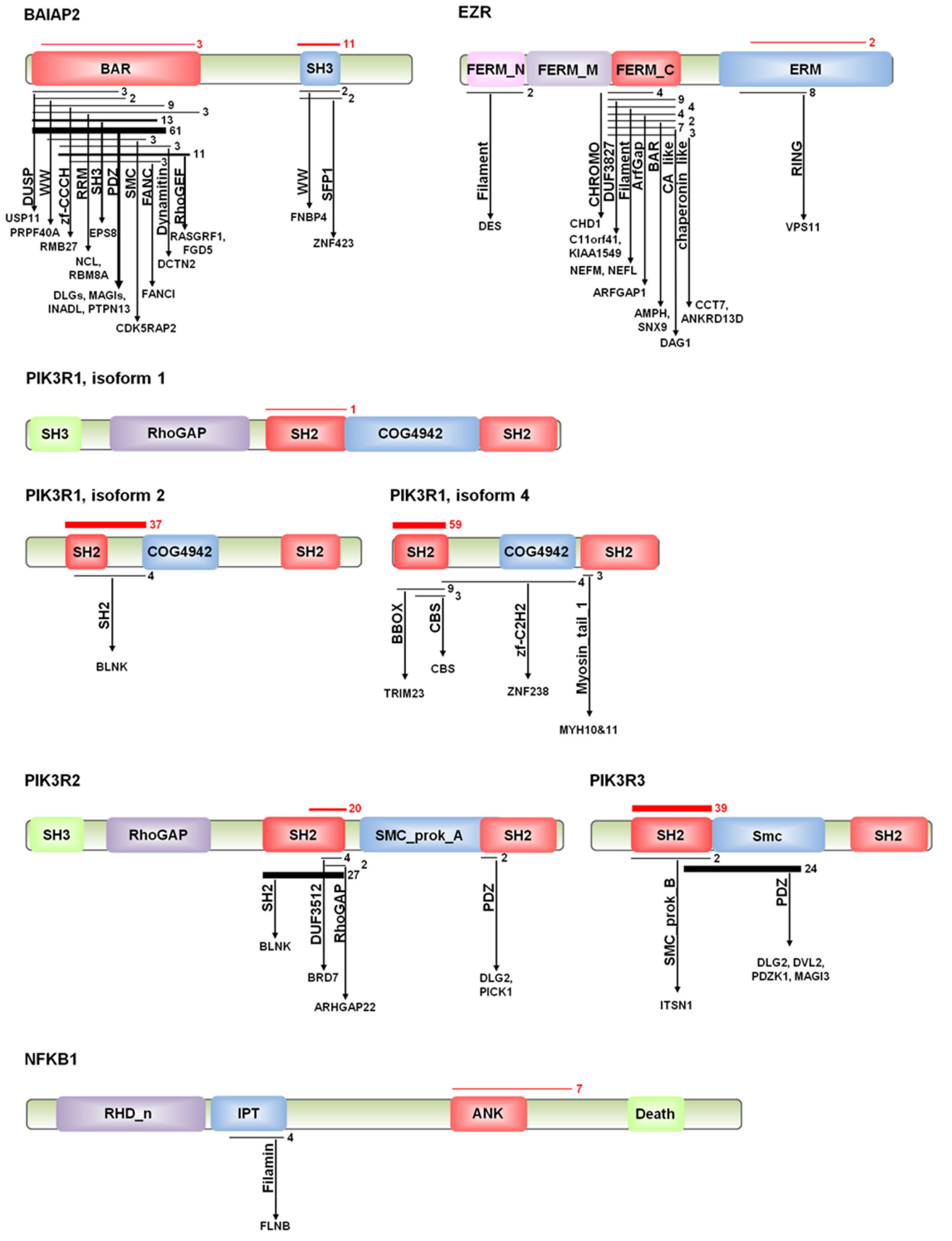
BAIAP2
BAR
SH3
DUSP
WW
zf-CCCH
RRM
SH3
PDZ
SMC
FANC
Dynamitin
RhoGEF
USP11
PRPF40A
RMB27
EPS8
NCL, RBM8A
RASGRF1, FGD5
DCTN2
DLGs, MAGIs, INADL, PTPN13
FANCI
CDK5RAP2
WW
SFP1
FNBP4
ZNF423
EZR
FERM_N
FERM_M
FERM_C
ERM
Filament
DES
CHROMO
DUF3827
Filament
ArfGap
BAR
CA like
chaperonin like
CHD1
C11orf41, KIAA1549
NEFM, NEFL
ARFGAP1
AMPH, SNX9
DAG1
CCT7, ANKRD13D
RING
VPS11
PIK3R1, isoform 1
SH3
RhoGAP
SH2
COG4942
SH2
PIK3R1, isoform 2
SH2
COG4942
SH2
SH2
BLNK
PIK3R1, isoform 4
SH2
COG4942
SH2
BBOX
CBS
zf-C2H2
Myosin tail 1
TRIM23
CBS
ZNF238
MYH10&11
PIK3R2
SH3
RhoGAP
SH2
SMC_prok_A
SH2
SH2
DUF3512
RhoGAP
BLNK
BRD7
ARHGAP22
PDZ
DLG2, PICK1
PIK3R3
SH2
Smc
SH2
SMC_prok_B
PDZ
ITSN1
DLG2, DVL2, PDZK1, MAGI3
NFKB1
RHD_n
IPT
ANK
Death
Filamin
FLNB

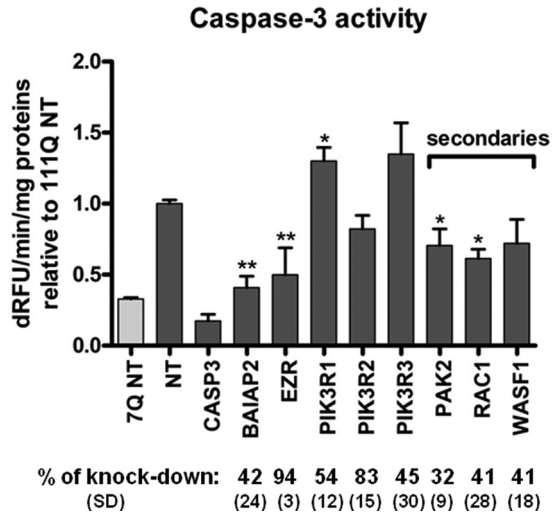

FIGURE 7. **Rho family GTPase signaling components modify mutant HTT-induced toxicity.** Caspase 3/7 activity following siRNA-mediated knockdown of Rho family GTPase signaling components in ST*Hdh*$^{111Q/111Q}$ cells ($n = 3$, *, p value<0.05; **, p value <0.01, t test). Data are represented as relative value to ST*Hdh*$^{111Q/111Q}$ treated with nontargeting siRNA (*NT*). Percent protein knockdown and standard deviations as determined by Western blot ($n = 3$) are indicated. *dRFU*, change in relative fluorescence units.

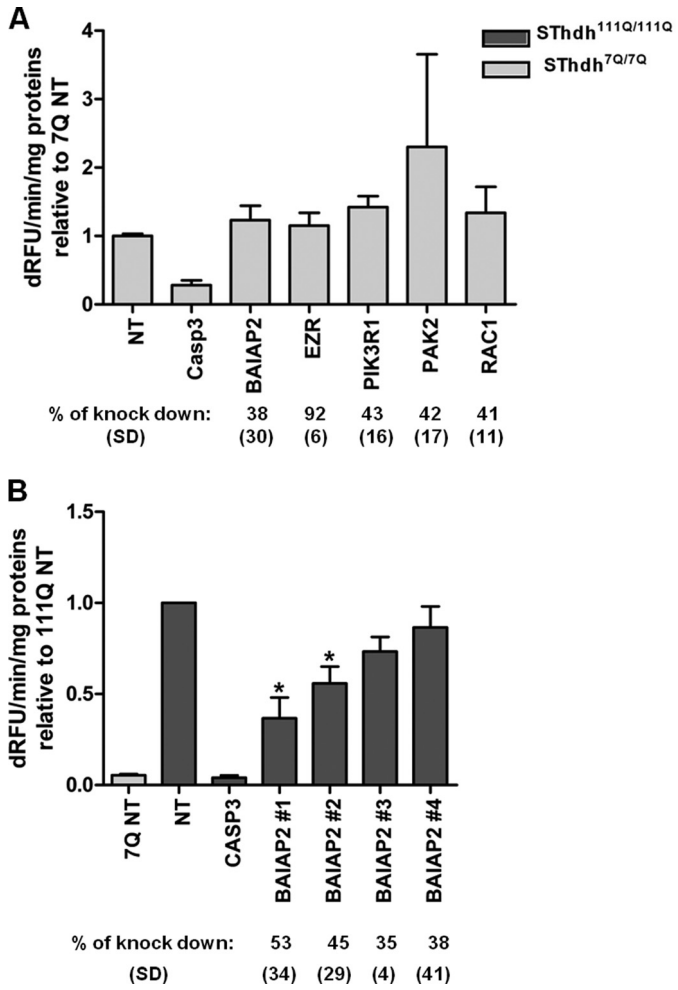

FIGURE 8. **Modifier effects of Rho family GTPase signaling components is specific for mutant HTT-induced toxicity.** *A,* caspase 3/7 assay following siRNA-mediated knockdown of Rho family GTPase signaling components in ST*Hdh*$^{7Q/7Q}$ cells ($n = 3$). Data are represented as relative to ST*Hdh*$^{7Q/7Q}$ treated with nontargeting siRNA (*NT*). Percent protein knockdown and standard deviations as determined by Western blot ($n = 3$) are indicated. *B,* caspase assay following BAIAP2 knockdown in ST*Hdh*$^{111Q/111Q}$ cells using individual siRNAs from deconvoluted pools ($n = 3$, *, p value<0.05, t test). Percent protein knockdown and standard deviations as determined by Western blot ($n = 3$) are indicated. *dRFU*, change in relative fluorescence units.

interact with HTT through their first SH2 domain. These data support a model of HTT acting as a large scaffolding protein interacting with multiple components of signaling and structural regulators of cytoskeletal and membrane remodeling factors at sites of cell movement.

Modifiers of HD Toxicity in the Rho GTPase Pathway—Our group and others have shown that physical partners of HTT are good candidates as potential modifiers of polyglutamine toxicity (15, 16, 71). As a first step of functional analysis, we asked whether manipulating levels of components of the Rho GTPases subnetwork were modifiers of mutant HTT cytotoxicity. To do this, we used an assay based on immortalized mouse striatal cell Hdh$^{7Q/7Q}$ and Hdh$^{111Q/111Q}$ lines (29) to evaluate the effect of knockdown of candidates on mutant HTT-specific caspase activation upon serum withdrawal (28).

Because it is a significantly enriched canonical pathway with a high levels of transcriptional dysregulation (Figs. 3 and 4), we decided to focus on components of the RhoGTPase signaling module for functional studies. This module contains seven primary HIPs (Fig. 4). Of these, NFKB1 and cAMP-response element-binding protein-binding protein are known to be modifiers of HTT toxicity (72, 73). These were not studied further. Of the remaining primary partners in this subnetwork, siRNA-mediated knockdown of three of the five tested proteins resulted in significant modification of toxicity in this cell model. Knockdown of BAIAP2 showed the most significant reduction of mutant HTT toxicity (Fig. 7), without any effect on caspase activity in the Hdh$^{7Q/7Q}$ cell line (Fig. 8). Intriguingly, expression of BAIAP2 is down-regulated in caudate of grade 0–2 HD patients. This could suggest a toxic role of the interaction between BAIAP2 and mutant HTT, with a compensatory effect of down-regulation in diseased neurons. Knockdown of EZR showed also a rescue effect on mutant HTT toxicity, without any effect on Hdh$^{7Q/7Q}$ cells. In this case, gene expression profiling of HD caudate showed an increase of EZR mRNA levels, suggesting that expression of EZR could be detrimental for HD neurons. Knockdown of regulatory subunits of PI3K seemed to enhance mutant HTT toxicity, with a significant effect of PIK3R1 knockdown effect in Hdh$^{111Q/111Q}$ cells, without any effect on Hdh$^{7Q/7Q}$ cells.

FIGURE 6. **Domain-domain interactions of primary partners in the Rho signaling module.** Schematic representation of primary partners of HTT from Rho GTPase signaling pathway. *Rectangles* and *associated labels* indicate conserved domains identified from Y2H sequence analysis. *Horizontal black lines* indicate the coverage of the domain by positive clone sequences; *numbers* to right of *black lines* and *thickness* indicate the number of independent Y2H observations. *Arrows* indicate interactions with other conserved domains (*vertical labels*) contained in interacting proteins of family members (*horizontal labels*). *Red lines* indicate coverage of positive sequence for HTT interaction regions. *Thickness* and *numbers* to right indicate number of independent observations of Y2H interaction of protein with HTT.

EZR, BAIAP2, and PI3K proteins are keys components of the signaling pathway through Rho family GTPases, but they are also involved in actin cytoskeletal organization and are present in the IPA actin cytoskeleton signaling pathway (Fig. 4). We examined secondary partners that were common between these two modules and asked whether they could modulate mutant HTT toxicity in striatal cell lines. PAK2 (p21-activated kinase 2) is a serine/threonine kinase that links small GTPases CDC42 and RAC1 to cytoskeleton reorganization (74). siRNA-mediated knockdown of RAC1 and PAK2 showed significant reduction of mutant HTT toxicity, without any effect on caspase activity in the $Hdh^{7Q/7Q}$ cell line. Overall, the observed suppressor effect of knockdown of RAC1 and PAK2 (and WASF1 which trended toward suppression) confirmed the involvement of BAIAP2 and EZR in mediating mutant HTT toxicity.

We then examined the functional significance of the interaction between HTT and Rho GTPase pathway members. Out of the numerous cell processes requiring components of this signaling pathway, cell migration, cell adhesion, and neurite outgrowth were of particular interest in regard to HD. One of the first molecular steps for these cellular processes is structural reorganization of the plasma membrane. Various plasma membrane structures, including invaginations (caveolae and clathrin-coated pits) and membrane protrusions, such as lamellipodia and filopodia, are involved in cell morphogenesis, endocytosis, cell migration, and neuritogenesis. Filopodia are cylindrical extensions of the plasma membrane that contain bundles of parallel actin filaments at their core (75). Filopodia are thought to act as sensors, probing their microenvironment and regulating cell protrusion and cell migration in response to extracellular cues. Key components of focal adhesions, such as integrin, cadherin, PTK2 (focal adhesion kinase), and Talin, are found in the tips of filopodia (76, 77). These cytoskeletal-membrane structures are necessary for neurite formation and outgrowth in cortical neurons (78, 79), as well as synaptogenesis (80). It has been shown that inhibition of Rac1 GTPase function decreases the number of axonal filopodia as well as at growth cone formation in sensory neurons, whereas inhibition of Cdc42 function inhibits filopodia formation only at growth cones (81). In these filopodial structures, BAIAP2 plays a central role as a linker between actin filaments, through its IMD domain and plasma membrane (82), and has been shown to regulate filopodia formation (47).

We confirmed the binary physical interaction between BAIAP2 and HTT observed with Y2H using co-immunoprecipitation methods. Using HEK293T cells overexpressing an HTT fragment (1–558) fused to GFP and BAIAP2 fused to V5 tag, we observed co-immunoprecipitation of normal (23Q) and mutant (135Q) HTT with BAIAP2 (Fig. 9*A*). We were also able to show a reciprocal co-immunoprecipitation of BAIAP2 with HTT fragment (Fig. 9*B*). Moreover, using NIH-3T3 cells, we showed that both nonexpanded and mutant HTT co-localized with BAIAP2 and filamentous actin at the tip of filopodial structures (Fig. 9*C*).

We next investigated the function of HTT in filopodia formation in the NIH-3T3 cell model. We co-transfected mouse fibroblasts with full-length HTT, normal (17Q), or mutant (138Q), or an empty vector control, along with V5-tagged BAIAP2 or V5-tagged LacZ (control). We observed that ectopic expression of BAIAP2 led to a significant increase in the number of actin-positive filopodia in NIH-3T3 cells when co-transfected with empty control. Overexpression of normal full-length HTT did not interfere with BAIAP2-induced increase of filopodia. However, expression of mutant HTT completely abolished this effect (Fig. 10*A*). This result suggests that the presence of mutant HTT inhibits the induction of filopodia formation by BAIAP2. Additionally, we showed that siRNA-mediated knockdown of BAIAP2 decreased the number of filopodia-like protrusions in mouse embryonic fibroblasts, without any effect of normal HTT overexpression (Fig. 10*B*). The presence of mutant HTT showed a trend to abolish this decrease. Filopodia are dynamic structures; elongation and retraction of the finger-like sensors are not yet completely understood. Rho family members have been shown to be involved in both formation and stabilization of these structures, and it would be of great interest to study dynamics of filopodia *in vitro* and *in vivo*, particularly at the neuronal, axonal, and synaptic level. These experiments demonstrate that huntingtin interacts both physically and genetically with the filopodial protein BAIAP2. Furthermore, mutant HTT can interfere with the ability of BAIAP2 to modulate filopodial morphogenesis.

DISCUSSION

Here, we describe HDNet, a protein interaction network that provides a genome-scale resource for elucidating normal functions of HTT, novel pathogenic mechanisms of mutant HTT, as well as deeper mechanistic insights into known pathways affected in HD. Partners of HTT identified in our screen, at both primary and secondary levels of interaction, showed enhanced interconnectivity as compared with other proteins in the context of HPRD, an independently derived and curated reference protein interaction network. We demonstrated that this connectivity is not due to node degree effects or annotation biases in HPRD. We conclude that independent validation of enhanced connectivity of HDNet arises from shared functional properties relevant to the functions of HTT as well as the pathogenic process in Huntington disease.

HDNet is significantly enriched in proteins that function in pathways known to be involved in HD, such as protein homeostasis, cytoskeleton, and vesicle trafficking (Fig. 3). These pathways were recently discovered and described as preferentially enriched in HTT partners from two interaction screens by affinity purification followed by mass spectrometry from brain of HD mouse models (14, 17). Here, we demonstrate that expanding the HD network with secondary interacting partners and combining enriched functional modules with gene expression dysregulation data from human brain tissue highlights signaling by Rho family GTPases and actin remodeling as being processes in HTT function and HD pathogenesis.

HDNet is a protein interaction network defined at the protein domain resolution. Identification of binding domain underlying protein interaction networks enhances our mechanistic understanding of how normal and pathological mechanisms may operate at the molecular level (83). This study used a Y2H method based on construction of binding domain and

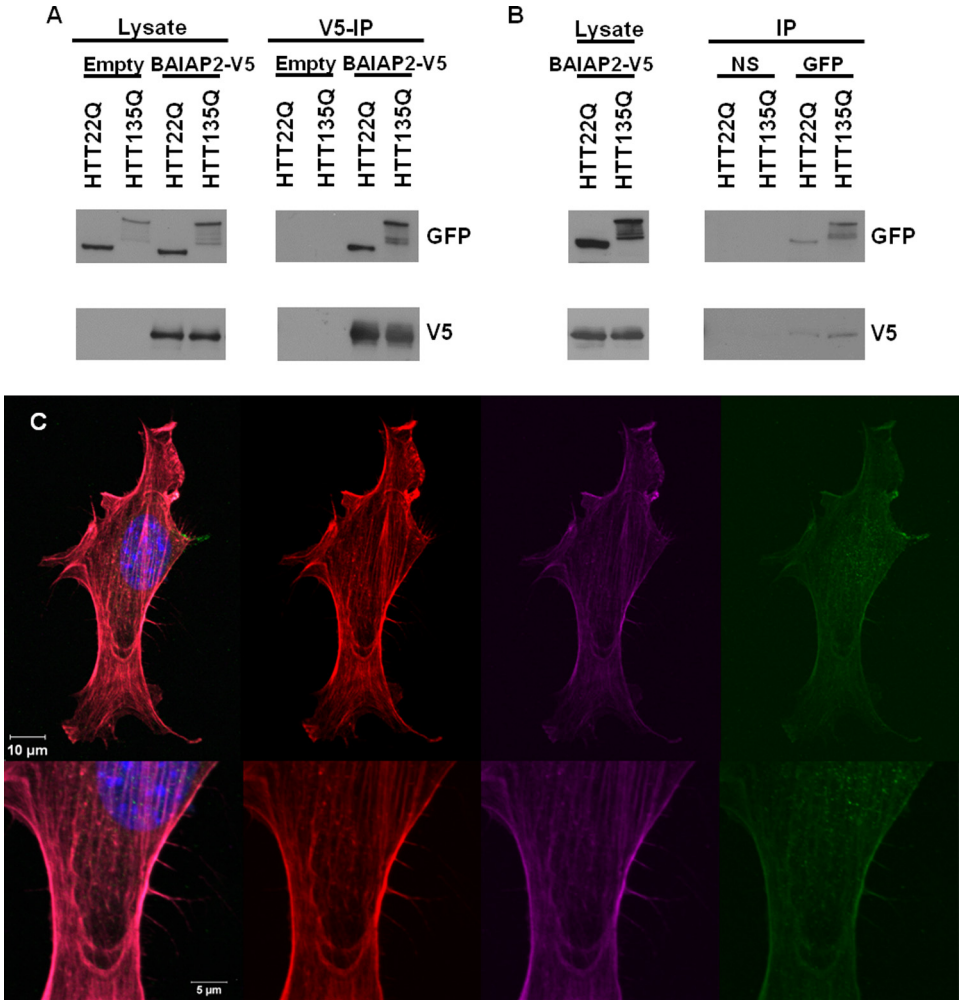

FIGURE 9. **HTT and BAIAP2 interact and co-localize in cells.** *A,* co-immunoprecipitation of GFP-tagged HTT fragments with V5-tagged BAIAP2 expressed in HEK293T cells. BAIAP2 was immunoprecipitated with anti-V5, and HTT was probed with a GFP antibody. A lysate transfected with empty vector was performed in parallel to confirm a specific protein interaction. 10% of input for each protein lysate (*left*) and immunoprecipitation (*IP*) results (*right*) are shown for each protein. *B,* reciprocal co-immunoprecipitation of V5-tagged BAIAP2 with GFP-tagged HTT. HTT was immunoprecipitated with anti-GFP. A native IgG pulldown was performed as a control (*NS*). *C,* co-localization (*left panel*) in actin-positive (*red, center left*) filopodia of BAIAP2 (*purple, center right*) and HTT (*green, right*) in NIH-3T3 cells. Nuclei were labeled with DAPI (*blue*).

activation domain libraries from cDNA fragments. Therefore, interactions reported here are between protein fragments rather than between full-length proteins (16, 21). In many cases these fragments were shown to contain specific conserved protein domains (as defined by the NCBI conserved domain database). Knowledge of specific domain-domain interactions provides a higher resolution understanding of how specific proteins are interacting with HTT itself as well as HTT binding partners. With regard to HD pathogenesis, identification of binding domains of HTT partners is of high interest. Some studies suggest that the normal role of polyQ regions in proteins would be to stabilize PPI, and expansion of polyQ could have a deleterious effect through a gain of abnormal interactions or impairments of protein interaction dynamics (84). Recently, the role of the proline-rich region of HTT has been highlighted in different studies. Intrabodies targeting PRR were shown to reduce toxicity of mutant HTT and increase turnover of mutant HTT (85). It was also shown that deletion of the PRR domain in full-length HTT caused late onset learning and memory deficits in transgenic mice (86). This suggests that protein interaction with the PRR domain of HTT can affect both its normal and toxic activities as well as turnover. Partners of HTT containing SH3 or WW domains in the binding sequences could thus represent an interesting group of modifiers. We also note that a number of proteins with SH3 domains are involved in cell motility pathways. These are SRGAP1, SRGAP2, SRGAP3, and BAIAP2.

Based on analysis of canonical pathways represented in HDNet and gene expression changes observed in HD brain, we focused on RhoGTPase signaling to validate a specific functional module as being involved in HTT function and toxicity. The potent loss-of-function suppression of HTT toxicity observed in ST*Hdh*$^{111Q/111Q}$ cells upon knockdown of BAIAP2 further focused our attention on filopodia components as modifiers of mutant HTT toxicity in cell models. These structures are essential for cell adhesion, cell migration, and neurite outgrowth (87). Here, we show that expression of mutant HTT impairs BAIAP2-induced filopodia formation. This phenomenon is observed for induction of filopodia formation following BAIAP2 overexpression, as well as a decrease of formation of

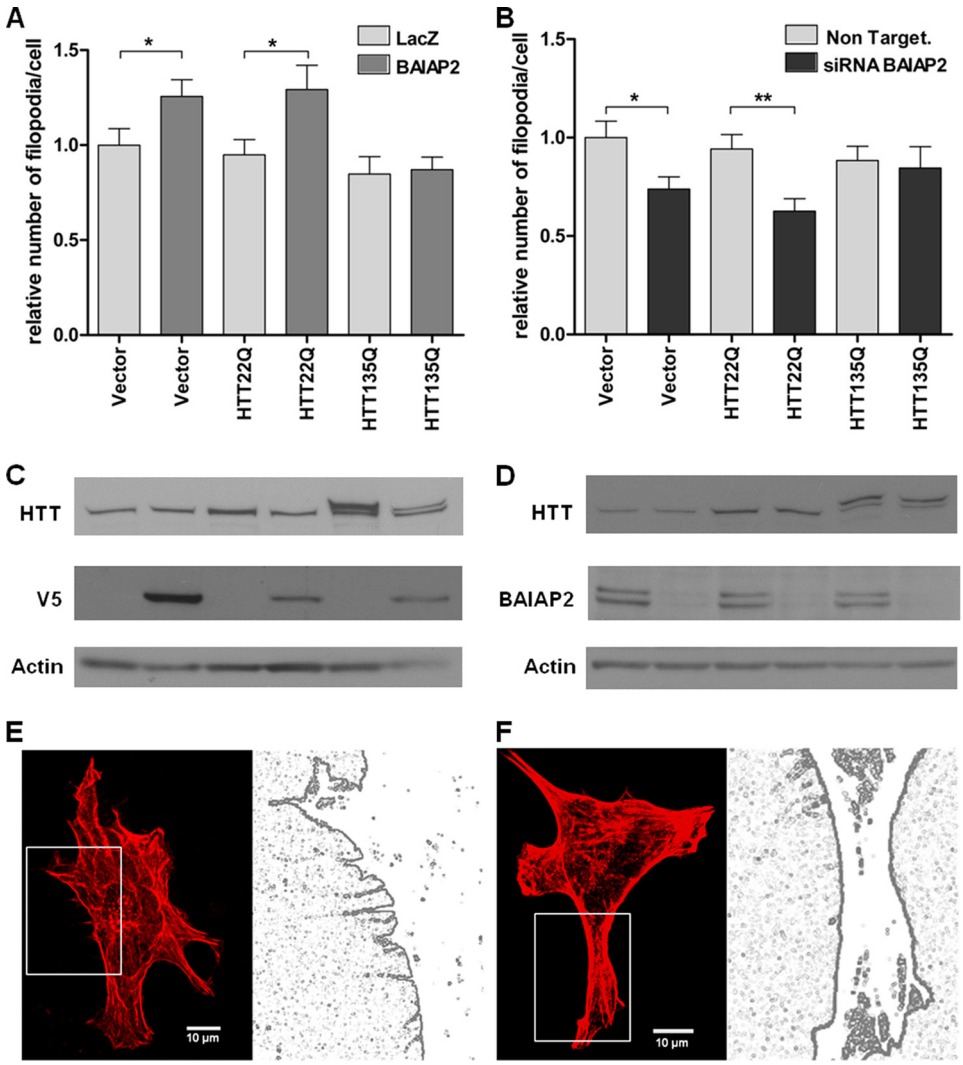

FIGURE 10. **Mutant HTT interferes with BAIAP2-induced filopodia formation.** *A,* NIH-3T3 cells were co-transfected with V5-tagged BAIAP2 or V5-tagged LacZ (control) along with full-length HTT (17Q) or HTT (138Q) or with an empty vector (control). Cells were fixed and stained with rhodamine-phalloidin, anti-V5, and anti-HTT. The number of actin-positive filopodia were counted in V5- and in HTT-positive cells, 15 cells per experiment with $n = 3$ (*, p value<0.05, t test). The relative numbers of filopodia in each condition are indicated. *B,* NIH-3T3 cells were co-transfected with BAIAP2 siRNA or nontargeting siRNA (control) along with full-length HTT (17Q), or HTT (138Q), or with an empty vector as (control). Cells were fixed and stained with rhodamine-phalloidin and anti-HTT. Number of actin-positive filopodia were counted in HTT-positive cells, 15 cells per experiment with $n = 3$ (*, p value<0.05; **, p value<0.01, t test). The relative numbers of filopodia in each condition are indicated. *C* and *D,* expression levels of BAIAP2 and HTT were analyzed by immunoblotting with indicated antibodies, using β-actin as a loading control, for overexpression (*C*) and knockdown (*D*) of BAIAP2. *E* and *F,* representative images of rhodamine-phalloidin labeled cells co-transfected with BAIAP2 and HTT 17Q (*E*) or 138Q (*F*), and their respective digitized images.

these structures following knockdown of BAIAP2. This suggests that mutant HTT can impair dynamic regulation of filopodia by BAIAP2. The regulation of BAIAP2-induced filopodial formation remains to be elucidated, as well as the specific involvement of this process in neuron-specific pathways. BAIAP2 is also a binding partner of PDZ domain-containing proteins such as DGL-4 (PSD-95) in the postsynaptic density indicating that the HTT-BAIAP2 interaction may influence both pre- and post-synaptic processes (88, 89). BAIAP2 has also has been shown to interact with ATN1 (atrophin-1), the protein responsible for DRPLA, a polyQ expansion disease with pathological and clinical similarities to HD (90). Identifying the protein composition of filopodia neurons affected in HD, and deciphering the involvement of HTT in these dynamic structures could help elucidate novel mechanisms of neuronal dysfunction. In human brain, previous studies showed marked morphological changes in dendritic structures and branching of medium spiny neurons in post-mortem HD brain (91, 92). Our data indicate that dynamic organization of neuronal processes as well as sites of cell-cell contacts may be a primary pathogenic mechanism in HD. Furthermore, we provide evidence that components of the Rho GTPase signaling cascade such as BAIAP2 can be directly affected by mutant HTT and are therefore candidates for HTT-mediated defects in cell morphology. The protein machinery regulating cytoskeleton-membrane interactions and filopodia formation represents key targets for further studies with regard to neurodevelopmental pathways and synaptic homeostasis in Huntington disease.

REFERENCES

1. The Huntington's Disease Collaborative Research Group (1993) A novel gene containing a trinucleotide repeat that is expanded and unstable on

Huntington's disease chromosomes. *Cell* **72,** 971–983
2. Reiner, A., Albin, R. L., Anderson, K. D., D'Amato, C. J., Penney, J. B., and Young, A. B. (1988) Differential loss of striatal projection neurons in Huntington disease. *Proc. Natl. Acad. Sci. U.S.A.* **85,** 5733–5737
3. Walker, F. O. (2007) Huntington's disease. *Lancet* **369,** 218–228
4. Borrell-Pagès, M., Zala, D., Humbert, S., and Saudou, F. (2006) Huntington's disease: from huntingtin function and dysfunction to therapeutic strategies. *Cell. Mol. Life Sci.* **63,** 2642–2660
5. Zuccato, C., Valenza, M., and Cattaneo, E. (2010) Molecular mechanisms and potential therapeutical targets in Huntington's disease. *Physiol. Rev.* **90,** 905–981
6. Wellington, C. L., Ellerby, L. M., Gutekunst, C. A., Rogers, D., Warby, S., Graham, R. K., Loubser, O., van Raamsdonk, J., Singaraja, R., Yang, Y. Z., Gafni, J., Bredesen, D., Hersch, S. M., Leavitt, B. R., Roy, S., Nicholson, D. W., and Hayden, M. R. (2002) Caspase cleavage of mutant huntingtin precedes neurodegeneration in Huntington's disease. *J. Neurosci.* **22,** 7862–7872
7. Graham, R. K., Deng, Y., Slow, E. J., Haigh, B., Bissada, N., Lu, G., Pearson, J., Shehadeh, J., Bertram, L., Murphy, Z., Warby, S. C., Doty, C. N., Roy, S., Wellington, C. L., Leavitt, B. R., Raymond, L. A., Nicholson, D. W., and Hayden, M. R. (2006) Cleavage at the caspase-6 site is required for neuronal dysfunction and degeneration due to mutant huntingtin. *Cell* **125,** 1179–1191
8. Ratovitski, T., Gucek, M., Jiang, H., Chighladze, E., Waldron, E., D'Ambola, J., Hou, Z., Liang, Y., Poirier, M. A., Hirschhorn, R. R., Graham, R., Hayden, M. R., Cole, R. N., and Ross, C. A. (2009) Mutant huntingtin N-terminal fragments of specific size mediate aggregation and toxicity in neuronal cells. *J. Biol. Chem.* **284,** 10855–10867
9. Sun, B., Fan, W., Balciunas, A., Cooper, J. K., Bitan, G., Steavenson, S., Denis, P. E., Young, Y., Adler, B., Daugherty, L., Manoukian, R., Elliott, G., Shen, W., Talvenheimo, J., Teplow, D. B., Haniu, M., Haldankar, R., Wypych, J., Ross, C. A., Citron, M., and Richards, W. G. (2002) Polyglutamine repeat length-dependent proteolysis of huntingtin. *Neurobiol. Dis.* **11,** 111–122
10. Boutell, J. M., Thomas, P., Neal, J. W., Weston, V. J., Duce, J., Harper, P. S., and Jones, A. L. (1999) Aberrant interactions of transcriptional repressor proteins with the Huntington's disease gene product, huntingtin. *Hum. Mol. Genet.* **8,** 1647–1655
11. Holbert, S., Denghien, I., Kiechle, T., Rosenblatt, A., Wellington, C., Hayden, M. R., Margolis, R. L., Ross, C. A., Dausset, J., Ferrante, R. J., and Néri, C. (2001) The Gln-Ala repeat transcriptional activator CA150 interacts with huntingtin: neuropathologic and genetic evidence for a role in Huntington's disease pathogenesis. *Proc. Natl. Acad. Sci. U.S.A.* **98,** 1811–1816
12. Steffan, J. S., Kazantsev, A., Spasic-Boskovic, O., Greenwald, M., Zhu, Y. Z., Gohler, H., Wanker, E. E., Bates, G. P., Housman, D. E., and Thompson, L. M. (2000) The Huntington's disease protein interacts with p53 and CREB-binding protein and represses transcription. *Proc. Natl. Acad. Sci. U.S.A.* **97,** 6763–6768
13. Caviston, J. P., Ross, J. L., Antony, S. M., Tokito, M., and Holzbaur, E. L. (2007) Huntingtin facilitates dynein/dynactin-mediated vesicle transport. *Proc. Natl. Acad. Sci. U.S.A.* **104,** 10045–10050
14. Culver, B. P., Savas, J. N., Park, S. K., Choi, J. H., Zheng, S., Zeitlin, S. O., Yates, J. R., 3rd, and Tanese, N. (2012) Proteomic analysis of wild-type and mutant huntingtin-associated proteins in mouse brains identifies unique interactions and involvement in protein synthesis. *J. Biol. Chem.* **287,** 21599–21614
15. Goehler, H., Lalowski, M., Stelzl, U., Waelter, S., Stroedicke, M., Worm, U., Droege, A., Lindenberg, K. S., Knoblich, M., Haenig, C., Herbst, M., Suopanki, J., Scherzinger, E., Abraham, C., Bauer, B., Hasenbank, R., Fritzsche, A., Ludewig, A. H., Büssow, K., Buessow, K., Coleman, S. H., Gutekunst, C. A., Landwehrmeyer, B. G., Lehrach, H., and Wanker, E. E. (2004) A protein interaction network links GIT1, an enhancer of huntingtin aggregation, to Huntington's disease. *Mol. Cell* **15,** 853–865
16. Kaltenbach, L. S., Romero, E., Becklin, R. R., Chettier, R., Bell, R., Phansalkar, A., Strand, A., Torcassi, C., Savage, J., Hurlburt, A., Cha, G. H., Ukani, L., Chepanoske, C. L., Zhen, Y., Sahasrabudhe, S., Olson, J., Kurschner, C., Ellerby, L. M., Peltier, J. M., Botas, J., and Hughes, R. E. (2007) Huntingtin interacting proteins are genetic modifiers of neurodegeneration. *PLoS Genet.* **3,** e82
17. Shirasaki, D. I., Greiner, E. R., Al-Ramahi, I., Gray, M., Boontheung, P., Geschwind, D. H., Botas, J., Coppola, G., Horvath, S., Loo, J. A., and Yang, X. W. (2012) Network organization of the huntingtin proteomic interactome in mammalian brain. *Neuron* **75,** 41–57
18. Bell, R., Hubbard, A., Chettier, R., Chen, D., Miller, J. P., Kapahi, P., Tarnopolsky, M., Sahasrabuhde, S., Melov, S., and Hughes, R. E. (2009) A human protein interaction network shows conservation of aging processes between human and invertebrate species. *PLoS Genet.* **5,** e1000414
19. Bandyopadhyay, S., Chiang, C. Y., Srivastava, J., Gersten, M., White, S., Bell, R., Kurschner, C., Martin, C., Smoot, M., Sahasrabudhe, S., Barber, D. L., Chanda, S. K., and Ideker, T. (2010) A human MAP kinase interactome. *Nat. Methods* **7,** 801–805
20. Ge, H., Walhout, A. J., and Vidal, M. (2003) Integrating 'omic' information: a bridge between genomics and systems biology. *Trends Genet.* **19,** 551–560
21. LaCount, D. J., Vignali, M., Chettier, R., Phansalkar, A., Bell, R., Hesselberth, J. R., Schoenfeld, L. W., Ota, I., Sahasrabudhe, S., Kurschner, C., Fields, S., and Hughes, R. E. (2005) A protein interaction network of the malaria parasite *Plasmodium falciparum*. *Nature* **438,** 103–107
22. Shannon, P., Markiel, A., Ozier, O., Baliga, N. S., Wang, J. T., Ramage, D., Amin, N., Schwikowski, B., and Ideker, T. (2003) Cytoscape: a software environment for integrated models of biomolecular interaction networks. *Genome Res.* **13,** 2498–2504
23. Keshava Prasad, T. S., Goel, R., Kandasamy, K., Keerthikumar, S., Kumar, S., Mathivanan, S., Telikicherla, D., Raju, R., Shafreen, B., Venugopal, A., Balakrishnan, L., Marimuthu, A., Banerjee, S., Somanathan, D. S., Sebastian, A., Rani, S., Ray, S., Harrys Kishore, C. J., Kanth, S., Ahmed, M., Kashyap, M. K., Mohmood, R., Ramachandra, Y. L., Krishna, V., Rahiman, B. A., Mohan, S., Ranganathan, P., Ramabadran, S., Chaerkady, R., and Pandey, A. (2009) Human Protein Reference Database–2009 update. *Nucleic Acids Res.* **37,** D767–D772
24. Hodges, A., Strand, A. D., Aragaki, A. K., Kuhn, A., Sengstag, T., Hughes, G., Elliston, L. A., Hartog, C., Goldstein, D. R., Thu, D., Hollingsworth, Z. R., Collin, F., Synek, B., Holmans, P. A., Young, A. B., Wexler, N. S., Delorenzi, M., Kooperberg, C., Augood, S. J., Faull, R. L., Olson, J. M., Jones, L., and Luthi-Carter, R. (2006) Regional and cellular gene expression changes in human Huntington's disease brain. *Hum. Mol. Genet.* **15,** 965–977
25. Kuhn, A., Goldstein, D. R., Hodges, A., Strand, A. D., Sengstag, T., Kooperberg, C., Becanovic, K., Pouladi, M. A., Sathasivam, K., Cha, J. H., Hannan, A. J., Hayden, M. R., Leavitt, B. R., Dunnett, S. B., Ferrante, R. J., Albin, R., Shelbourne, P., Delorenzi, M., Augood, S. J., Faull, R. L., Olson, J. M., Bates, G. P., Jones, L., and Luthi-Carter, R. (2007) Mutant huntingtin's effects on striatal gene expression in mice recapitulate changes observed in human Huntington's disease brain and do not differ with mutant huntingtin length or wild-type huntingtin dosage. *Hum. Mol. Genet.* **16,** 1845–1861
26. Miller, J. P., Yates, B. E., Al-Ramahi, I., Berman, A. E., Sanhueza, M., Kim, E., de Haro, M., DeGiacomo, F., Torcassi, C., Holcomb, J., Gafni, J., Mooney, S. D., Botas, J., Ellerby, L. M., and Hughes, R. E. (2012) A genome-scale RNA-interference screen identifies RRAS signaling as a pathologic feature of Huntington's disease. *PLoS Genet.* **8,** e1003042
27. Campeau, E., Ruhl, V. E., Rodier, F., Smith, C. L., Rahmberg, B. L., Fuss, J. O., Campisi, J., Yaswen, P., Cooper, P. K., and Kaufman, P. D. (2009) A versatile viral system for expression and depletion of proteins in mammalian cells. *PLoS One* **4,** e6529
28. Miller, J. P., Holcomb, J., Al-Ramahi, I., de Haro, M., Gafni, J., Zhang, N., Kim, E., Sanhueza, M., Torcassi, C., Kwak, S., Botas, J., Hughes, R. E., and Ellerby, L. M. (2010) Matrix metalloproteinases are modifiers of huntingtin proteolysis and toxicity in Huntington's disease. *Neuron* **67,** 199–212
29. Trettel, F., Rigamonti, D., Hilditch-Maguire, P., Wheeler, V. C., Sharp, A. H., Persichetti, F., Cattaneo, E., and MacDonald, M. E. (2000) Dominant phenotypes produced by the HD mutation in STHdh(Q111) striatal cells. *Hum. Mol. Genet.* **9,** 2799–2809
30. Barabási, A. L., Gulbahce, N., and Loscalzo, J. (2011) Network medicine: a network-based approach to human disease. *Nat. Rev. Genet.* **12,** 56–68
31. Yuan, T. L., and Cantley, L. C. (2008) PI3K pathway alterations in cancer:

variations on a theme. *Oncogene* **27,** 5497–5510
32. Rommel, C., Camps, M., and Ji, H. (2007) PI3Kδ and PI3Kγ: partners in crime in inflammation in rheumatoid arthritis and beyond? *Nat. Rev. Immunol.* **7,** 191–201
33. Lee, J. Y., Kim, Y. R., Park, J., and Kim, S. (2012) Inositol polyphosphate multikinase signaling in the regulation of metabolism. *Ann. N.Y. Acad. Sci.* **1271,** 68–74
34. Chong, Z. Z., Shang, Y. C., Wang, S., and Maiese, K. (2012) A critical kinase cascade in neurological disorders: PI 3-K, Akt, and mTOR. *Future Neurol.* **7,** 733–748
35. Ravikumar, B., Vacher, C., Berger, Z., Davies, J. E., Luo, S., Oroz, L. G., Scaravilli, F., Easton, D. F., Duden, R., O'Kane, C. J., and Rubinsztein, D. C. (2004) Inhibition of mTOR induces autophagy and reduces toxicity of polyglutamine expansions in fly and mouse models of Huntington disease. *Nat. Genet.* **36,** 585–595
36. Seredenina, T., and Luthi-Carter, R. (2012) What have we learned from gene expression profiles in Huntington's disease? *Neurobiol. Dis.* **45,** 83–98
37. Borgonovo, J. E., Troncoso, M., Lucas, J. J., and Sosa, M. A. (2013) Mutant huntingtin affects endocytosis in striatal cells by altering the binding of AP-2 to membranes. *Exp. Neurol.* **241,** 75–83
38. Trushina, E., Singh, R. D., Dyer, R. B., Cao, S., Shah, V. H., Parton, R. G., Pagano, R. E., and McMurray, C. T. (2006) Mutant huntingtin inhibits clathrin-independent endocytosis and causes accumulation of cholesterol *in vitro* and *in vivo*. *Hum. Mol. Genet.* **15,** 3578–3591
39. Lange, A., Wickström, S. A., Jakobson, M., Zent, R., Sainio, K., and Fässler, R. (2009) Integrin-linked kinase is an adaptor with essential functions during mouse development. *Nature* **461,** 1002–1006
40. Qin, J., and Wu, C. (2012) ILK: a pseudokinase in the center stage of cell-matrix adhesion and signaling. *Curr. Opin. Cell Biol.* **24,** 607–613
41. Bauer, P. O., Wong, H. K., Oyama, F., Goswami, A., Okuno, M., Kino, Y., Miyazaki, H., and Nukina, N. (2009) Inhibition of Rho kinases enhances the degradation of mutant huntingtin. *J. Biol. Chem.* **284,** 13153–13164
42. Shao, J., Welch, W. J., and Diamond, M. I. (2008) ROCK and PRK-2 mediate the inhibitory effect of Y-27632 on polyglutamine aggregation. *FEBS Lett.* **582,** 1637–1642
43. De Las Rivas, J., and Fontanillo, C. (2010) Protein-protein interactions essentials: key concepts to building and analyzing interactome networks. *PLoS Comput. Biol.* **6,** e1000807
44. Buchsbaum, R. J. (2007) Rho activation at a glance. *J. Cell Sci.* **120,** 1149–1152
45. Miki, H., Yamaguchi, H., Suetsugu, S., and Takenawa, T. (2000) IRSp53 is an essential intermediate between Rac and WAVE in the regulation of membrane ruffling. *Nature* **408,** 732–735
46. Mattila, P. K., Pykäläinen, A., Saarikangas, J., Paavilainen, V. O., Vihinen, H., Jokitalo, E., and Lappalainen, P. (2007) Missing-in-metastasis and IRSp53 deform PI(4,5)P2-rich membranes by an inverse BAR domain-like mechanism. *J. Cell Biol.* **176,** 953–964
47. Robens, J. M., Yeow-Fong, L., Ng, E., Hall, C., and Manser, E. (2010) Regulation of IRSp53-dependent filopodial dynamics by antagonism between 14-3-3 binding and SH3-mediated localization. *Mol. Cell. Biol.* **30,** 829–844
48. Neisch, A. L., and Fehon, R. G. (2011) Ezrin, Radixin and Moesin: key regulators of membrane-cortex interactions and signaling. *Curr. Opin. Cell Biol.* **23,** 377–382
49. Marsick, B. M., Roche, F. K., and Letourneau, P. C. (2012) Repulsive axon guidance cues ephrin-A2 and slit3 stop protrusion of the growth cone leading margin concurrently with inhibition of ADF/cofilin and ERM proteins. *Cytoskeleton* **69,** 496–505
50. Marchler-Bauer, A., Lu, S., Anderson, J. B., Chitsaz, F., Derbyshire, M. K., DeWeese-Scott, C., Fong, J. H., Geer, L. Y., Geer, R. C., Gonzales, N. R., Gwadz, M., Hurwitz, D. I., Jackson, J. D., Ke, Z., Lanczycki, C. J., Lu, F., Marchler, G. H., Mullokandov, M., Omelchenko, M. V., Robertson, C. L., Song, J. S., Thanki, N., Yamashita, R. A., Zhang, D., Zhang, N., Zheng, C., and Bryant, S. H. (2011) CDD: a conserved domain database for the functional annotation of proteins. *Nucleic Acids Res.* **39,** D225–D229
51. Bedford, M. T., Reed, R., and Leder, P. (1998) WW domain-mediated interactions reveal a spliceosome-associated protein that binds a third class of proline-rich motif: the proline glycine and methionine-rich motif. *Proc. Natl. Acad. Sci. U.S.A.* **95,** 10602–10607
52. Chow, W. N., Luk, H. W., Chan, H. Y., and Lau, K. F. (2012) Degradation of mutant huntingtin via the ubiquitin/proteasome system is modulated by FE65. *Biochem. J.* **443,** 681–689
53. Faber, P. W., Barnes, G. T., Srinidhi, J., Chen, J., Gusella, J. F., and MacDonald, M. E. (1998) Huntingtin interacts with a family of WW domain proteins. *Hum. Mol. Genet.* **7,** 1463–1474
54. Passani, L. A., Bedford, M. T., Faber, P. W., McGinnis, K. M., Sharp, A. H., Gusella, J. F., Vonsattel, J. P., and MacDonald, M. E. (2000) Huntingtin's WW domain partners in Huntington's disease post-mortem brain fulfill genetic criteria for direct involvement in Huntington's disease pathogenesis. *Hum. Mol. Genet.* **9,** 2175–2182
55. Jiang, Y. J., Che, M. X., Yuan, J. Q., Xie, Y. Y., Yan, X. Z., and Hu, H. Y. (2011) Interaction with polyglutamine-expanded huntingtin alters cellular distribution and RNA processing of huntingtin yeast two-hybrid protein A (HYPA). *J. Biol. Chem.* **286,** 25236–25245
56. Zheng, S., Ghitani, N., Blackburn, J. S., Liu, J. P., and Zeitlin, S. O. (2012) A series of N-terminal epitope tagged Hdh knock-in alleles expressing normal and mutant huntingtin: their application to understanding the effect of increasing the length of normal Huntingtin's polyglutamine stretch on CAG140 mouse model pathogenesis. *Mol. Brain* **5,** 28
57. Allen, M., Friedler, A., Schon, O., and Bycroft, M. (2002) The structure of an FF domain from human HYPA/FBP11. *J. Mol. Biol.* **323,** 411–416
58. Bedford, M. T., and Leder, P. (1999) The FF domain: a novel motif that often accompanies WW domains. *Trends Biochem. Sci.* **24,** 264–265
59. Chiang, M. C., Chen, C. M., Lee, M. R., Chen, H. W., Chen, H. M., Wu, Y. S., Hung, C. H., Kang, J. J., Chang, C. P., Chang, C., Wu, Y. R., Tsai, Y. S., and Chern, Y. (2010) Modulation of energy deficiency in Huntington's disease via activation of the peroxisome proliferator-activated receptor γ. *Hum. Mol. Genet.* **19,** 4043–4058
60. Huang, H., Li, L., Wu, C., Schibli, D., Colwill, K., Ma, S., Li, C., Roy, P., Ho, K., Songyang, Z., Pawson, T., Gao, Y., and Li, S. S. (2008) Defining the specificity space of the human SRC homology 2 domain. *Mol. Cell. Proteomics* **7,** 768–784
61. Morton, C. J., and Campbell, I. D. (1994) SH3 domains. Molecular 'Velcro'. *Curr. Biol.* **4,** 615–617
62. Chuang, J. Z., Zhou, H., Zhu, M., Li, S. H., Li, X. J., and Sung, C. H. (2002) Characterization of a brain-enriched chaperone, MRJ, that inhibits Huntingtin aggregation and toxicity independently. *J. Biol. Chem.* **277,** 19831–19838
63. Lu, B., Al-Ramahi, I., Valencia, A., Wang, Q., Berenshteyn, F., Yang, H., Gallego-Flores, T., Ichcho, S., Lacoste, A., Hild, M., Difiglia, M., Botas, J., and Palacino, J. (2013) Identification of NUB1 as a suppressor of mutant Huntington toxicity via enhanced protein clearance. *Nat. Neurosci.* **16,** 562–570
64. Muchowski, P. J., Schaffar, G., Sittler, A., Wanker, E. E., Hayer-Hartl, M. K., and Hartl, F. U. (2000) Hsp70 and hsp40 chaperones can inhibit self-assembly of polyglutamine proteins into amyloid-like fibrils. *Proc. Natl. Acad. Sci. U.S.A.* **97,** 7841–7846
65. Suetsugu, S., Toyooka, K., and Senju, Y. (2010) Subcellular membrane curvature mediated by the BAR domain superfamily proteins. *Semin. Cell Dev. Biol.* **21,** 340–349
66. Disanza, A., Mantoani, S., Hertzog, M., Gerboth, S., Frittoli, E., Steffen, A., Berhoerster, K., Kreienkamp, H. J., Milanesi, F., Di Fiore, P. P., Ciliberto, A., Stradal, T. E., and Scita, G. (2006) Regulation of cell shape by Cdc42 is mediated by the synergic actin-bundling activity of the Eps8-IRSp53 complex. *Nat. Cell Biol.* **8,** 1337–1347
67. Krugmann, S., Jordens, I., Gevaert, K., Driessens, M., Vandekerckhove, J., and Hall, A. (2001) Cdc42 induces filopodia by promoting the formation of an IRSp53:Mena complex. *Curr. Biol.* **11,** 1645–1655
68. Lim, K. B., Bu, W., Goh, W. I., Koh, E., Ong, S. H., Pawson, T., Sudhaharan, T., and Ahmed, S. (2008) The Cdc42 effector IRSp53 generates filopodia by coupling membrane protrusion with actin dynamics. *J. Biol. Chem.* **283,** 20454–20472
69. Nakagawa, H., Miki, H., Nozumi, M., Takenawa, T., Miyamoto, S., Wehland, J., and Small, J. V. (2003) IRSp53 is colocalised with WAVE2 at the tips of protruding lamellipodia and filopodia independently of Mena.

J. Cell Sci. **116,** 2577–2583
70. Suetsugu, S., Murayama, K., Sakamoto, A., Hanawa-Suetsugu, K., Seto, A., Oikawa, T., Mishima, C., Shirouzu, M., Takenawa, T., and Yokoyama, S. (2006) The RAC binding domain/IRSp53-MIM homology domain of IRSp53 induces RAC-dependent membrane deformation. *J. Biol. Chem.* **281,** 35347–35358
71. Li, S. H., and Li, X. J. (2004) Huntingtin-protein interactions and the pathogenesis of Huntington's disease. *Trends Genet.* **20,** 146–154
72. Jiang, H., Poirier, M. A., Liang, Y., Pei, Z., Weiskittel, C. E., Smith, W. W., DeFranco, D. B., and Ross, C. A. (2006) Depletion of CBP is directly linked with cellular toxicity caused by mutant huntingtin. *Neurobiol. Dis.* **23,** 543–551
73. Yu, Z., Zhou, D., Cheng, G., and Mattson, M. P. (2000) Neuroprotective role for the p50 subunit of NF-κB in an experimental model of Huntington's disease. *J. Mol. Neurosci.* **15,** 31–44
74. Manser, E., Leung, T., Salihuddin, H., Zhao, Z. S., and Lim, L. (1994) A brain serine/threonine protein kinase activated by Cdc42 and Rac1. *Nature* **367,** 40–46
75. Mattila, P. K., and Lappalainen, P. (2008) Filopodia: molecular architecture and cellular functions. *Nat. Rev. Mol. Cell Biol.* **9,** 446–454
76. Galbraith, C. G., Yamada, K. M., and Galbraith, J. A. (2007) Polymerizing actin fibers position integrins primed to probe for adhesion sites. *Science* **315,** 992–995
77. Vasioukhin, V., Bauer, C., Yin, M., and Fuchs, E. (2000) Directed actin polymerization is the driving force for epithelial cell-cell adhesion. *Cell* **100,** 209–219
78. Dent, E. W., Kwiatkowski, A. V., Mebane, L. M., Philippar, U., Barzik, M., Rubinson, D. A., Gupton, S., Van Veen, J. E., Furman, C., Zhang, J., Alberts, A. S., Mori, S., and Gertler, F. B. (2007) Filopodia are required for cortical neurite initiation. *Nat. Cell Biol.* **9,** 1347–1359
79. Kwiatkowski, A. V., Rubinson, D. A., Dent, E. W., Edward van Veen, J., Leslie, J. D., Zhang, J., Mebane, L. M., Philippar, U., Pinheiro, E. M., Burds, A. A., Bronson, R. T., Mori, S., Fässler, R., and Gertler, F. B. (2007) Ena/VASP is Required for neuritogenesis in the developing cortex. *Neuron* **56,** 441–455
80. Menna, E., Fossati, G., Scita, G., and Matteoli, M. (2011) From filopodia to synapses: the role of actin-capping and anti-capping proteins. *Eur. J. Neurosci.* **34,** 1655–1662
81. Spillane, M., Ketschek, A., Donnelly, C. J., Pacheco, A., Twiss, J. L., and Gallo, G. (2012) Nerve growth factor-induced formation of axonal filopodia and collateral branches involves the intra-axonal synthesis of regulators of the actin-nucleating Arp2/3 complex. *J. Neurosci.* **32,** 17671–17689
82. Millard, T. H., Bompard, G., Heung, M. Y., Dafforn, T. R., Scott, D. J., Machesky, L. M., and Fütterer, K. (2005) Structural basis of filopodia formation induced by the IRSp53/MIM homology domain of human IRSp53. *EMBO J.* **24,** 240–250
83. Ngounou Wetie, A. G., Sokolowska, I., Woods, A. G., Roy, U., Deinhardt, K., and Darie, C. C. (2013) Protein-protein interactions: switch from classical methods to proteomics and bioinformatics-based approaches. *Cell. Mol. Life Sci.* **71,** 205–228
84. Schaefer, M. H., Wanker, E. E., and Andrade-Navarro, M. A. (2012) Evolution and function of CAG/polyglutamine repeats in protein-protein interaction networks. *Nucleic Acids Res.* **40,** 4273–4287
85. Southwell, A. L., Khoshnan, A., Dunn, D. E., Bugg, C. W., Lo, D. C., and Patterson, P. H. (2008) Intrabodies binding the proline-rich domains of mutant huntingtin increase its turnover and reduce neurotoxicity. *J. Neurosci.* **28,** 9013–9020
86. Neveklovska, M., Clabough, E. B., Steffan, J. S., and Zeitlin, S. O. (2012) Deletion of the huntingtin proline-rich region does not significantly affect normal huntingtin function in mice. *J. Huntingtons Dis.* **1,** 71–87
87. Ahmed, S., Goh, W. I., and Bu, W. (2010) I-BAR domains, IRSp53 and filopodium formation. *Semin. Cell Dev. Biol.* **21,** 350–356
88. Hori, K., Yasuda, H., Konno, D., Maruoka, H., Tsumoto, T., and Sobue, K. (2005) NMDA receptor-dependent synaptic translocation of insulin receptor substrate p53 via protein kinase C signaling. *J. Neurosci.* **25,** 2670–2681
89. Soltau, M., Berhörster, K., Kindler, S., Buck, F., Richter, D., and Kreienkamp, H. J. (2004) Insulin receptor substrate of 53 kDa links postsynaptic shank to PSD-95. *J. Neurochem.* **90,** 659–665
90. Thomas, E. A., Foye, P. E., Alvarez, C. E., Usui, H., and Sutcliffe, J. G. (2001) Insulin receptor substrate protein p53 localization in rats suggests mechanism for specific polyglutamine neurodegeneration. *Neurosci. Lett.* **309,** 145–148
91. Ferrante, R. J., Kowall, N. W., and Richardson, E. P., Jr. (1991) Proliferative and degenerative changes in striatal spiny neurons in Huntington's disease: a combined study using the section-Golgi method and calbindin D28k immunocytochemistry. *J. Neurosci.* **11,** 3877–3887
92. Graveland, G. A., Williams, R. S., and DiFiglia, M. (1985) Evidence for degenerative and regenerative changes in neostriatal spiny neurons in Huntington's disease. *Science* **227,** 770–773